Fall 12-4-2015

# Visual Feedback System for Ultrasound Training

Saeideh Akbarisamani
saeideh.akbari.1985@gmail.com

# VISUAL FEEDBACK SYSTEM FOR ULTRASOUND TRAINING

by

Saeideh Akbarisamani

A THESIS

Presented to the Faculty of

The Graduate College at the University of Nebraska

In Partial Fulfillment of Requirements

For the Degree of Master of Science

Major: Mechanical Engineering & Applied Mechanics

Under the Supervision of Professors Jeff A. Hawks and Carl A. Nelson

Lincoln, Nebraska

December, 2015

VISUAL FEEDBACK SYSTEM FOR ULTRASOUND TRAINING

Saeideh Akbarisamani, M.S.

University of Nebraska, 2015

Adviser: Jeff Hawks and Carl Nelson

Astronauts returning from spaceflight have been found to exhibit many changes in their bodies such as intracranial pressure (ICP) increase similar to idiopathic intracranial hypertension, optic disk edema, vision change, back pain, optic nerve sheath distension, etc. Research shows that many changes in the body may occur in space because of microgravity. Different techniques have been used to measure changes in the body using ultrasound before, during, and after spaceflight. In most of these techniques, skilled technicians have been needed. Astronauts receive 40 hours of medical training. Part of that training is performing an ocular ultrasound to image the optic nerve and posterior globe. The astronauts are not skilled sonographers, which is why a device is necessary to assist with training.

This thesis presents the design and development of an ultrasound training system using force and orientation feedback, using a miniature load cell, a 3D-printed ultrasound probe holder, an accelerometer, and a LCD display. Design and implementation of the device are discussed. Ten different untrained users tested the device to see the efficacy of the device in ultrasound training purposes. The t-test calculated from the recorded data from experiments was 0.047 showing the significant difference of this device with having

real-time visual feedback compared to not having real-time feedback system used into current ultrasound protocol.

*"Truth is ever to be found in simplicity,*
*and not in the multiplicity and*
*confusion of things."*
Isaac Newton

*First of all, I would like to thank my research advisors and thesis committee members: Dr. Jeff Hawks, Dr. Carl Nelson, Dr. Shane Farritor, and Dr. Greg Bashford, who have dedicated their time and effort towards this project for their guidance and support. I would like to thank my colleagues and Biomedical Imaging and Biosignal Analysis (BIBA) Laboratory for their infinite support.*

*I would like to thank my fabulous husband, Babak. His infinite love, patience, and support have helped me to pursue my dreams.*

*Finally, I would like to thank my parents, my sisters, and my brothers for their continued support and encouragement over the years and their enthusiasm. I'm grateful for everything they have done.*

This research was performed under support provided by National Science Foundation and the NASA Nebraska Space Grant Consortium.

# Table of Contents

# List of Figures

# List of Tables

# Chapter 1: Introduction

Astronauts returning from spaceflight have been found to exhibit intracranial pressure increases similar to idiopathic intracranial hypertension. Research has shown that after going to space, many symptoms such as optic nerve sheath distension, posterior globe flattening, optic nerve protrusion, may occur depending on spaceflight duration. The study of visual acuity degradation is a new topic for researchers and helps them to find a way to prevent or reduce long-term consequences for these important problems [1].

Astronauts are expected to train for space flights in different areas. Space medical training has a significant impact on crew members' health and safety. They receive 40 hours of training in medical diagnosis and therapeutics, and a one-hour "hands-on" practice session before their flight [2]. Astronauts should be trained in ultrasonography to assist flight surgeons in diagnosing injuries or monitoring physiological changes during space flight due to microgravity environments. Observations of 7 astronauts after 6 months of spaceflight show that microgravity will cause disk edema, globe flattening, choroidal folds, "cotton wool" spots, nerve fiber layer thickening, and decreased near vision. Consequently, NASA began to collect data from magnetic resonance imaging (MRI), optical coherence tomography (OCT), and lumbar punctures (LP) before and after long duration space flights for astronauts to better understand the physiological changes caused by microgravity exposure [3]. A lot of astronauts have symptoms of headache, vomiting, nausea, fatigue, and lethargy when they face microgravity environments [4]. Therefore, monitoring these changes in the body is very important. Intracranial pressure (ICP) is the pressure of cerebrospinal fluid (CSF) that is surrounding the optic nerve and

central retinal artery [5, 6] and ICP is coupled with ocular hemodynamics. In [7, 8], they have used ultrasound to measure ocular hemodynamics to indirectly measure ICP using a noninvasive ICP measurement method based on a two-depth high-resolution transcranial Doppler insonation of the ophthalmic artery. Figure 1.1 illustrates optic disk edema during and after 10 days of returning from space flight captured from fundoscopy [9].

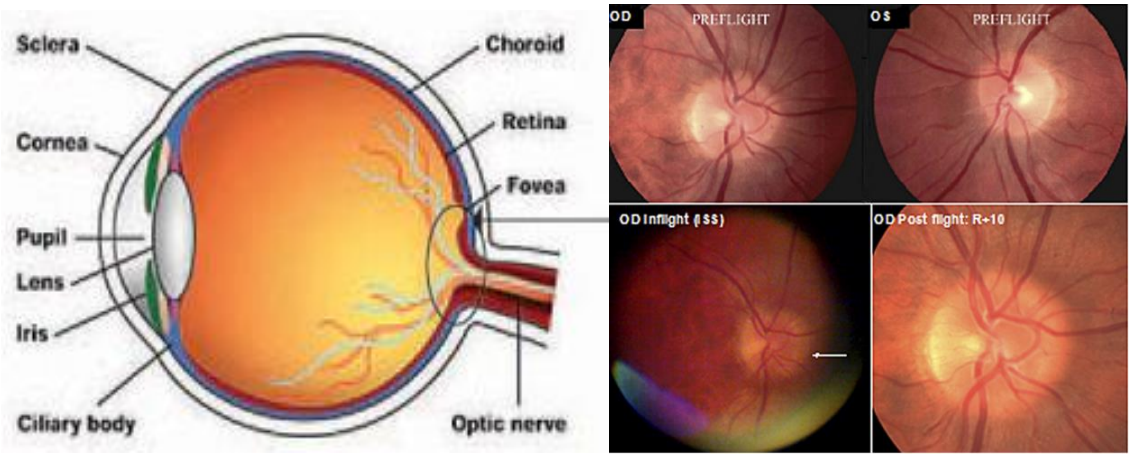


**Fig. 1.1: optic disk edema, normal eye schematic (left), preflight left and right posterior pole (right-top), during and after space flight posterior pole (right- bottom) [9].**

Also, there is possibility of distention in optic nerve sheath in microgravity conditions. Figure 1.2 shows a 12-mm distended optic nerve sheath after returning from space flight that bring possibility of intracranial pressure that is taken by ultrasound machine [10].

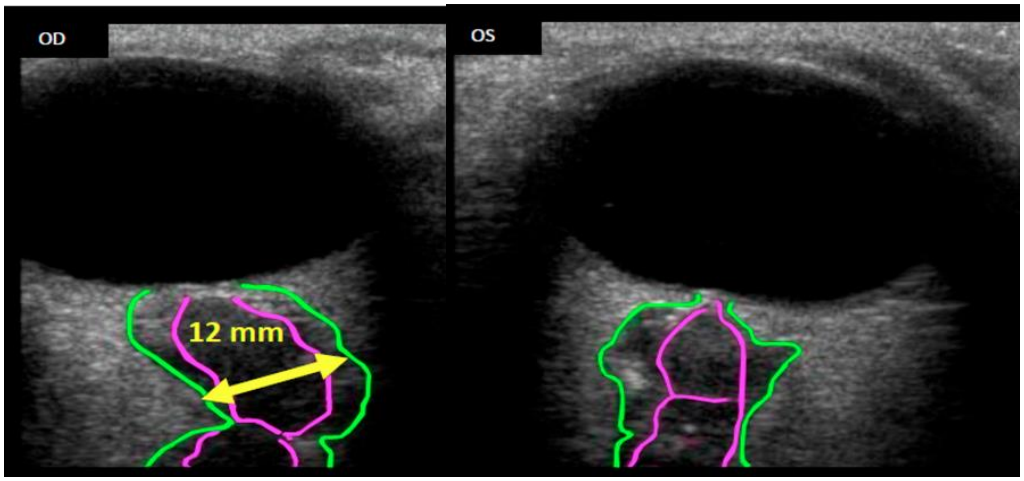


**Fig. 1.2: optic nerve sheath distension post flight (left), preflight (right) [10].**

Currently, physicians use ultrasound to get images of soft tissues in the body for diagnostic purposes. A technician holds the ultrasound probe on the patient's body aimed at the tissue of interest. Ultrasound uses high frequency sound waves and their echoes similar to some animals like whales and dolphins. When the technician holds the probe on the patient's body, the machine sends high-frequency sound pulses into the body. These waves go into the body and reflect back to the ultrasound device; the machine uses the patterns of reflected waves to reconstruct the tissue geometry [11]. Better imaging results and higher signal to noise ratio (SNR) correspond to consistent contact against the body. For imaging very soft tissues near the surface, such as the carotid artery, contact forces of up to 6.4 N are needed [12]. An untrained astronaut cannot efficiently create diagnostic quality images from ultrasonography, even with tele-mentoring guidance from a skilled sonographer on the ground; it would be even harder to take quality images in difficult circumstances such as injury and fatigue. Also, in microgravity environments, astronauts may face musculoskeletal fatigue in some areas in the body [13].

An automated feedback system prototype has been designed and developed for training astronauts to help them to improve the efficacy of their training and to be implemented into current training protocols. This thesis presents the design and development of the automated feedback system with force and orientation display. Also, the experiments and future work will be discussed.

# Chapter 2: Background

The importance of using ultrasound for different measurements and physiology monitoring will be described in this chapter. For achieving successful spaceflights, the health, safety, and levels of human performance are very important. Because physiological changes occur in different parts of the body such as musculoskeletal, cardiovascular, neurohormonal and the immune system, ultrasound has been used in space research to gain information related to these changes in the body. Martin et al. in [14] gives a brief description about the history of using ultrasound in space and discuss related applications. Some astronauts experience motion sickness, nasal congestion, vision changes, incontinence and urinary retention and back pain during spaceflight. However, they tend to feel more comfortable after several days of microgravity conditions. According to this paper there a lot of difficulties in using ultrasound during spaceflight, and the results may not be clear or precise. Also, there are some limitations for making equipment for research related to space, such as limited space, limited available power (28 V DC), ergonomic factors, material used, heat generation, and noise. So as an engineer to make equipment to be used during space flight, there should be some consideration of these factors. Some ultrasound equipment has been used such as Argument Centre National d'etude Spatiale (CNES) Matra Echograph PVH, American flight Echograph (AFE), ISS Human Research Facility ultrasound system (shown in Figure 2.1), and Hewlett Packard [14].

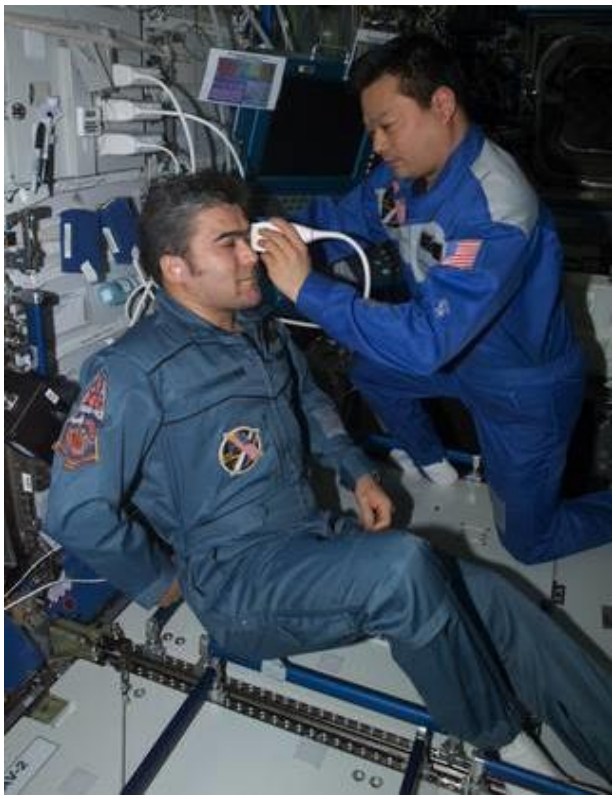

**Figure 2.1: Using the ADUM protocols, ISS Expedition Commander Leroy Chiao performs an ultrasound examination of the eye on Flight Engineer Salizhan Sharipov. (NASA)**

Microgravity plays an important role via loading, fluid shifts and lack of venous drainage. Researchers hypothesize that ICP increases due to the cephalad fluid shift and other physiological markers (i.e. optic nerve sheath distention, globe flattening). One of the big interests in the visual impairment/intracranial pressure (VIIP) risk is that changes in visual acuity did not return to normal after spaceflight. The anatomical changes in the eye seemed to be permanent. So, monitoring the changes in an astronaut's body during space flight using ultrasound is very important for researching diagnoses and treatments.

Cephalad fluid shits can be simulated without being in space using head-down tilt (HDT) bed rest. This study was performed on 8 healthy males who underwent HDT bed

rest for 30 days to show ICP adaptation using a non-invasive ICP measurement. In this study, researchers used a measurement technique to measure cranial oscillations before and at the end of this 30 days test and they collected data from pulse phase-locked loop (PPLL) output voltage and arterial blood pressure (BP). The results showed that the ICP amplitude decreased by 60% after 30 days. As a result, a cephalad-fluid shift plays a significant role in this study. Also, they showed that there are correlations between intracranial blood flow and tissue fluid during bed rest causing reduction of skull pulsation amplitudes, which are similar to being in an upright position [15].

ICP may increase if some changes happen in cerebrospinal fluid (CSF) dynamics, cerebral blood flow (CBF) and cerebral blood volume (CBV). There are different ways for measuring ICP such as using brain intraventricular and intraparenchymal catheter. Bhatia et. al. in [16] shows different ways of ICP monitoring and waveform analysis, and shows different techniques of cerebral blood flow assessment such as transcranial Doppler ultrasonography, laser Doppler and thermal diffusion flowmetry that is a non-invasive technique to calculate the blood flow in microcirculation. The result is that ICP monitoring and cerebral blood flow measurements using different techniques are necessary for patients with brain injuries, because they are at high risk of intracranial hypertension elevation [17]. Fogarty et al. [18] suggest that a technique for ICP monitoring is needed during spaceflight for achieving good results correlating visual impairment and ICP using ultrasonography. Masuda et al. in [19] developed a three-dimensional motion mechanism for an ultrasound probe controlled with two joysticks to capture images at a hospital when the device is located at home.

Vieyres et al. [20] developed an ultrasound probe handler that is a teleoperated robot, which can be used to take ultrasound images on astronauts or other remote patients with good quality and on any area of the body. The maximum applied force to the patient's skin is 15 N depending on the location of the body. In their paper they proposed a tele-echography project (TERESA) that gives astronauts a solution for getting ultrasound images with the quality of ground ultrasound images without having a technician present. Dulchavsky et al. in [21] describes using a spinal ultrasound technique during spaceflight, using real time data and methods to quantify the risk of spine problems by taking diagnostic quality images. They represent spinal ultrasound examination by the crewmembers during spaceflight.

In this chapter, the importance of measuring ICP using ultrasound during spaceflight has been targeted. The reason for choosing ICP is that ICP is very likely to cause harm if it rises too high, and it's very important to monitor this change. Currently, there is no handheld ultrasound probe handler with force measurement and orientation capabilities to be used during spaceflight, which would allow crew members to apply a steady and consistent force to the body. We designed and prototyped a small handheld device to be held by operators comfortably to get images from ultrasound probes in a precise and repeatable manner for both training and during missions. The TER system [22] has some advantages such as ability to use several control modes, impedance control, and the ability to adapt to the body shape. Another system was designed with accuracy of < 0.5 mm using a 10-22 MHz transducer using a 2 cm depth setting. In this system, temporal calibration is essential for finding the offset between two time stamps one is position sensor and the other one is B-scan. Also, spatial calibration (calibration on

the flat plane) for giving the size and location of the B-scan information was used in this system. In this study, it was necessary to have a very precise tissue-mimicking ultrasound phantom [23]. Another study researched and illustrated three methods of ultrasound transducer calibration including single point method, 2-D alignment method, and free hand method [24]. In [25], a system of using a comprehensive, multimedia, computer-based program was developed and tested for the first time in 2002 onboard the International Space Station (ISS) to capture images from abdominal, chest, thyroid gland, cardiovascular system (Figure 2.3 [26]) without the availability of an ultrasound specialist onboard. Guidance by a specialist from a remote site using cue cards with explanation of the system they use in ISS was provided. Figure 2.2 shows these cue cards. The cards contain mapping of the specific keyboard used for the ISS ultrasound machine, anatomical reference point for initial probe application, primary probe manipulation concepts, and terminology.

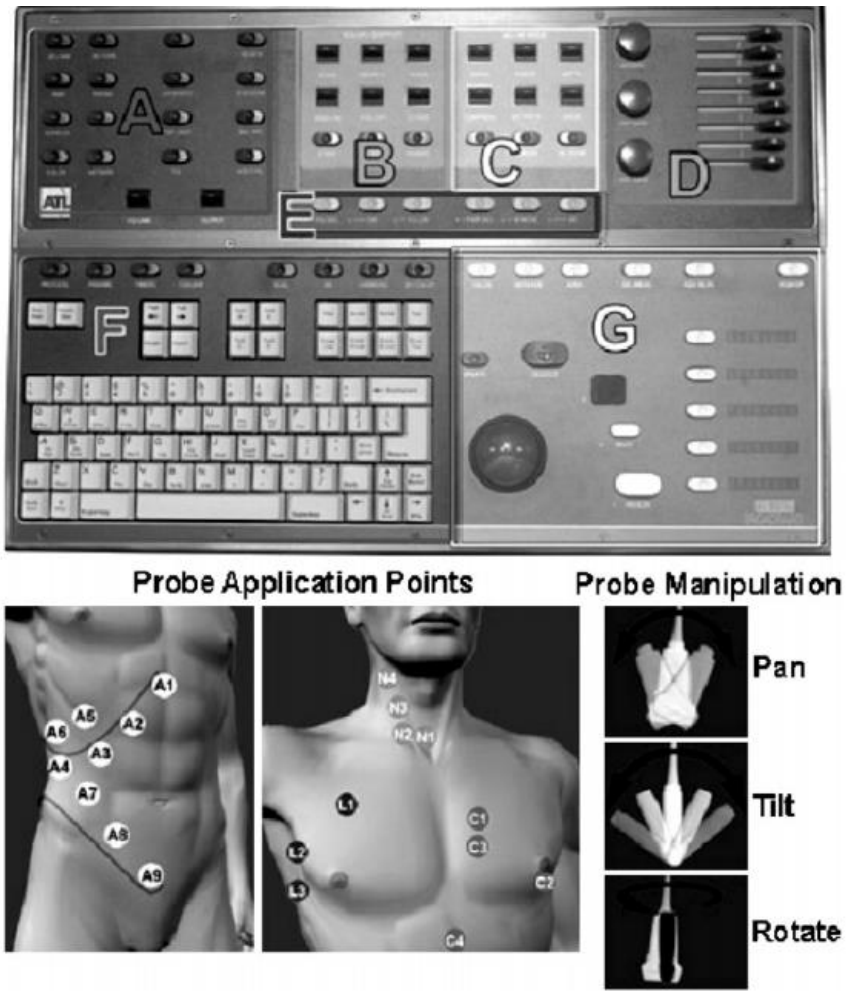


**Fig. 2.2: ISS cue card with mapping keyboard (top), initial probe application and probe movement (bottom) [26]**

**Fig. 2.3: First Remotely Guided Ultrasound Imaging on the ISS (2002) using cue cards [26]**

Also, an ultrasound probe holder has been made to control the ultrasound probe remotely with the lack of a specialist. Some of these devices were able to control the force applied to the patient's body, and some of them did not [19, 20]. Figure 2.4 and 2.5 show these remotely tele-echography systems.

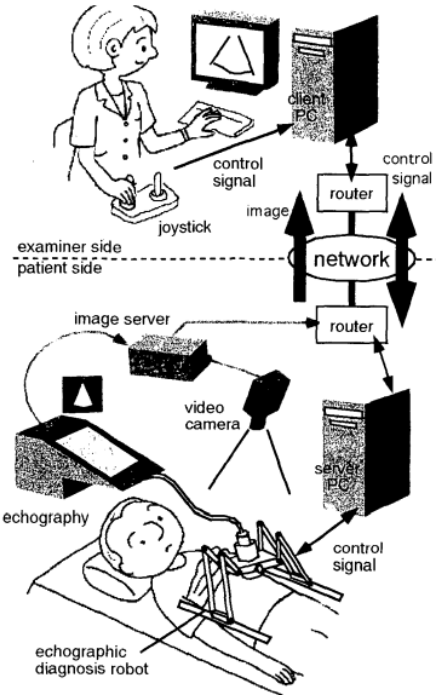


**Fig. 2.4: Remote Echography Diagnosis System (3 dimensional movable robot) [19,20]**

**Fig. 2.5: Tele-Echography (TERESA) [19,20]**

The limitation of using all of these systems to get quality images from ultrasonography is that these systems require a highly-skilled operator at the remote site to be always available. In most of them, there wasn't any real-time feedback about the amount of applied force, as well as the orientation of the probe. Using a two-axis joystick tele-echography system makes it difficult to control the device. In the TERESA project, there was a possibility of applying too much or too little force [19, 20, 25].

This thesis presents the design of a handheld ultrasound probe suited for the constraints of spaceflight. We first discuss the force display process, its operating principle, and the component selection for this subsystem. Then, we discuss the orientation display and its hardware components and circuit design. Finally, we discuss software and integration. Experiments are also presented to demonstrate the device capabilities.

# Chapter 3: Motivation

## *Section 3.1: Overview*

There are some assistive devices for holding ultrasound probes that are handheld for ultrasonography purposes, [7, 12, 13, 14, 19, and 20], with different advantages and disadvantages. One of their major disadvantages is that they are not adjustable for different types and sizes of ultrasound probes. Also, most of them are not able to control force applied to the body. Measuring applied force of the ultrasound probe on the body becomes very important to achieve good image quality, especially for operators with minimal training. Previous work in making devices to help astronauts to measure changes, which occur in the body during spaceflight in, has focused on various applications. Some of these are measuring applied force to the body. Some are fixed devices without measuring applied force to the body. The new design in this thesis is not a fixed device and can be moved to different locations because it is a small and portable device, which measures forces that are applied to the desired area in the body.

The system described in this thesis is adjustable for many different probes, providing easy interchange between probes. The software and hardware used also make it portable. The new system is able to give information on the orientation of the device and the amount of applied force to the body, which can facilitate getting good image data even when used by novice operators.

## *Section 3.2: Design Requirements*

Several factors should be considered when designing an automated feedback system for ultrasound training. The ability to measure the applied force to a certain area in the body, the ability to measure the orientation and position of the probe, and showing the output data on a LCD display are the main design requirements. Also, it should be small enough to hold it by the user comfortably.

The records from repeated measured deformation applied to the same tissue shows different results because of different applied force to the tissue [27]. Another study has been developed in making a hand-controller design for getting ultrasound images remotely. This design has a four-degree of freedom parallel mechanism. Its novelty is the ability for providing standard clinical motion for ultrasound imaging. Also, the design provided has a fixed center of motion for creating required ultrasound motions [28]. Figure 3.1 shows different ultrasound transducer motions. Figure 3.1.a shows linear motion and Figure 3.1.b-d show rotation of the transducer on the patient's body within a conical workspace with about 60 degrees vertex angle. Remaining in contact with the patient's body continuously for getting precise results is very important. The OTELO device has demonstrated that the ultrasound specialist can get the results from echography examination remotely with the help of paramedic using a six-degree of freedom design with 3-rotation access for the probe, and three translations [29]. Figure 3.2 shows the degree of freedom of ultrasound probe.

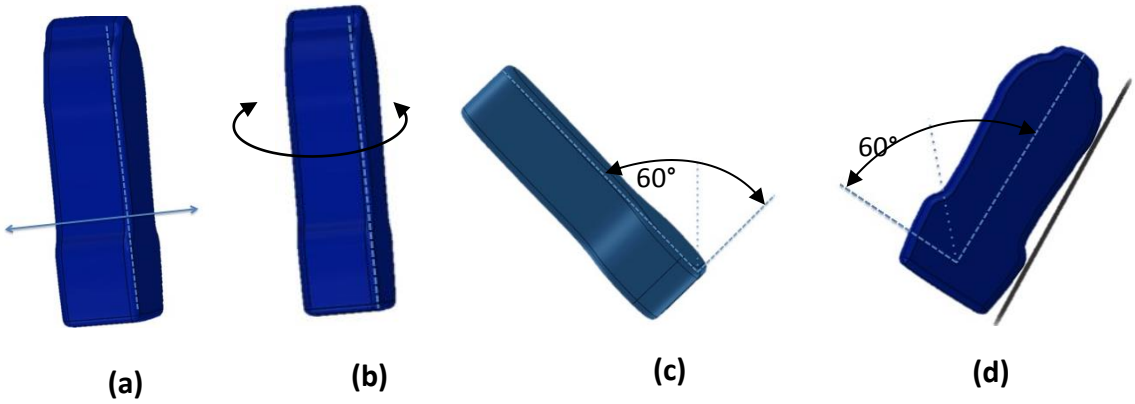


**Figure 3.1: Different ultrasound transducer motions. a) linear motion, b) spinning motion, c) pitch motion, d) yaw motion**

From all of these factors and observations a number of requirements for our system were derived:

- Size: user will hold the device on top of the patient's body in contact to the skin. For getting accurate results, the device should be small enough to be held by one hand comfortably.

- Force: the device we are going to design should be able to measure specific amount of forces for different parts of the body and show the data on a LCD. The following amount of contact force for a carotid artery ultrasound examination according to the orientation shown in Table 3.1 [30] and heart with assigned examination system [31] is considered.

- Orientation: the device should be able to help the user move the probe in a precise direction.

**Table 3.1: Maximum contact force [24]**

| Force (Carotid Artery) | | | Force (Cornea) | Force (Heart) |
|---|---|---|---|---|
| $F_x$ | $F_y$ | $F_z$ | 1.5-2.5N<br>0.337-0.562lb | 4.5N<br>1.012lb |
| 3.8N<br>0.854lb | 4.2N<br>0.944lb | 6.4N<br>1.438lb | | |

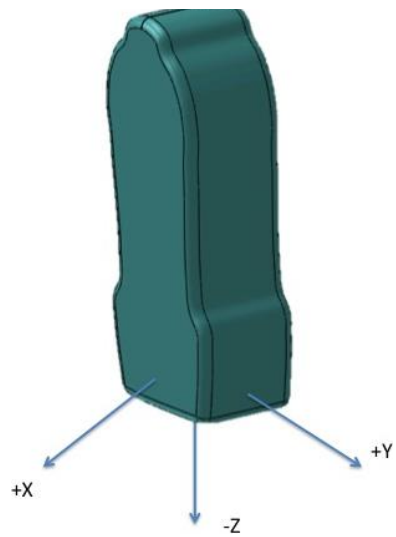


**Figure 3.2: Axis orientation on the assistive device**

The next chapter illustrates the design of a device to control the force, position, and orientation of the ultrasound probe when is applying to the body by the user. The system uses an accelerometer and a load cell installed on top of the device.

# Chapter 4: System Description

## *Section 4.1: Force Display*

This chapter describes the design of a handheld force and orientation device for holding different types of ultrasound probes for use in ultrasound training. A user holds the device, and a load cell is used to measure the contact force between the probe and the patient's body. The goal of the force measurement and display was to design a handheld device to help control the applied force to the patient's body. This section describes the design of a novel system to measure applied contact force to the body using a very small force sensor.

### *Section 4.1.1: Operating Principle*

The fundamental requirements named in the previous chapter (size, force, orientation) are applied in this design in the force and orientation feedback phase. The user holds a 3D-printed device made out of plastic. This device houses an ultrasound transducer, a load cell, and an Inertial Measurement Unit (IMU) for measuring orientation. Different types of ultrasound transducers can be placed inside of the device whenever needed according to the ultrasound training protocol. Specifications of transducers are shown in Table 4.1 [32]. Figure 4.1 shows Futek load cell mounting diagram.

**Table 4.1: ultrasound components used to be put in the device**

**(http://www.dwl.de/index.php?art_id=enen2540b8be4516e569539c0f5d8515)**

| | | |
|---|---|---|
|  | Doppler-BoxX by DWL Compumedics Gmbh | Possible to measure throughout the entire depth range. Flow direction and depth information are displayed in real time. |
|  | DopplerBox<br>DWL Ultrasound Probe<br>PW 2 | Frequency range of 2MHz |
|  | Siemens PH4-1 Transducer Probe | Frequency range of 1-4 MHz<br><br>Abdomen, Fetal Echo, OB/GYN |
|  | Siemens VF 7-3 Linear Ultrasound Transducer | Frequency range 3-7 MHz<br><br>Vascular/small parts |
|  | Siemens VF 13-5 Linear Array Ultrasound Probe | Frequency range of 5.0 to 13.0 MHz<br>Thyroid, Musculoskeletal, Breast |

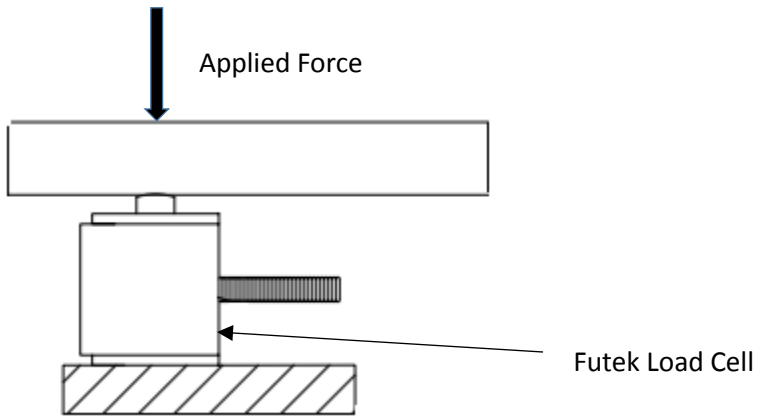


**Figure 4.1: load cell mounting diagram**

Figure 4.2 represents the operating principle of the design. The device is designed to have two small pieces connected by a hinge shown in the figure below such that forces from the user's hand are transferred through the load cell to determine the axial forces seen at the surface of the transducer. Figure 4.3 shows the free body diagram of the device. This figure also represents the equations involving reaction forces from the user's hand, hinge, load cell, and the patient's body. On one hand, the applied force by the user is equal to the difference of the force of the hinge and force of the load cell, and on the other hand, the reaction force from the body is equal to the difference of the force of the hinge and force of the load cell. This implies that all force applied to the device by the hand is transferred to the tissue. From the equations in Figure 4.3, $d_1$ is the distance between the hinge and load cell (13 mm) and $d_2$ is the distance between the hinge and the line of action of the user-applied force (41.15mm). $F_{LC}$ is the measured applied force by the load cell. From these equations $F_{body} = d_1/d_2\ F_{LC}$ where the distance ratio is 0.316. For example, if the force measured in the load cell is 13.345 N, the hand is applying (and the body is receiving) 4.23 N.

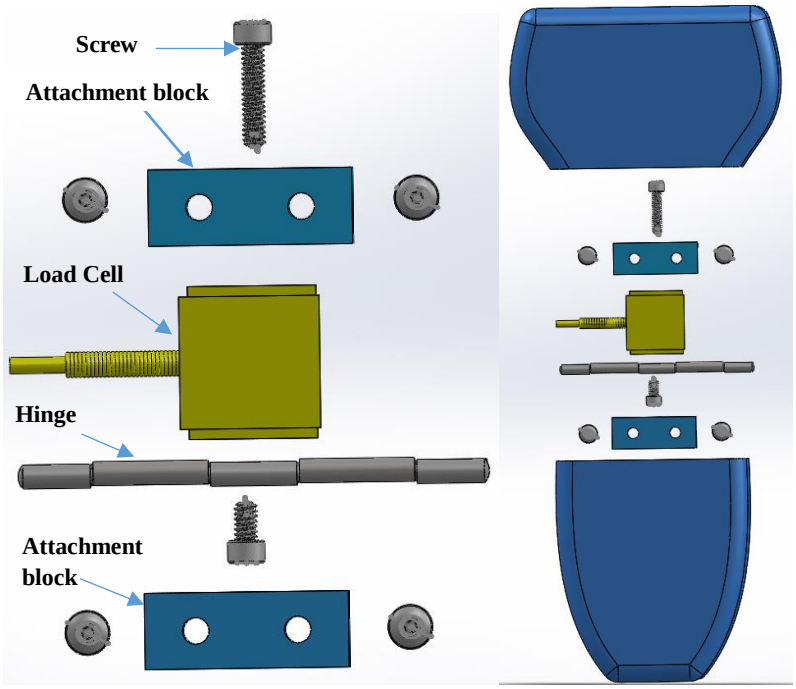


**Figure 4.2: Load cell operating principle**

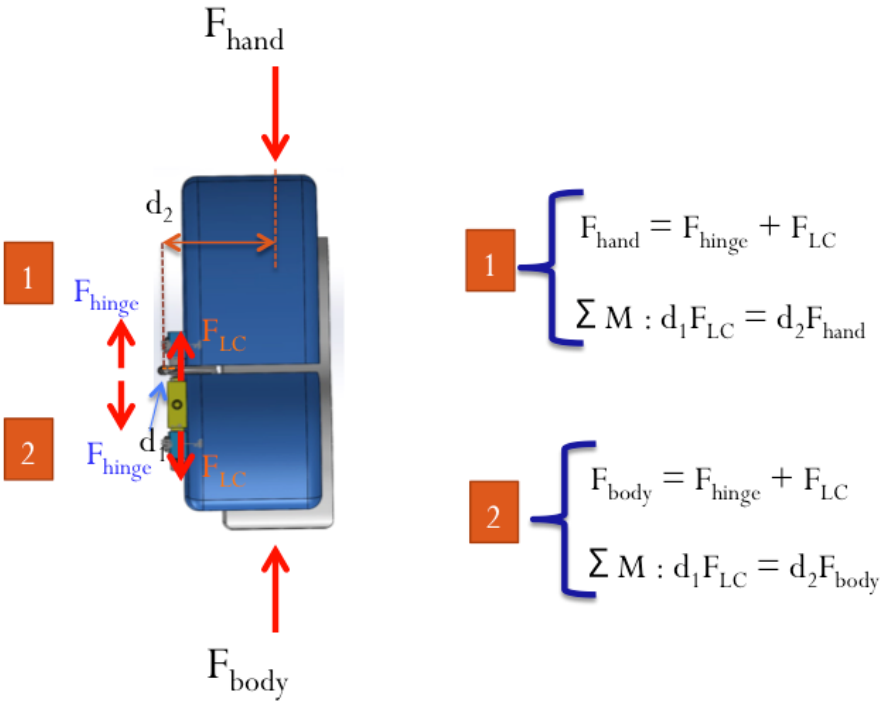


**Fig. 4.3: Device free body diagram**

At this point the final design of the ultrasound transducer holder is shown in Figure 4.4. a-e. Part a shows back of the device including load cell, hinge, screws, and the load cell attachment blocks. Parts b-e show different transducers with fasteners needed to hold and fix them into the device. Figure 4.5 shows the prototypes of the probe holders.

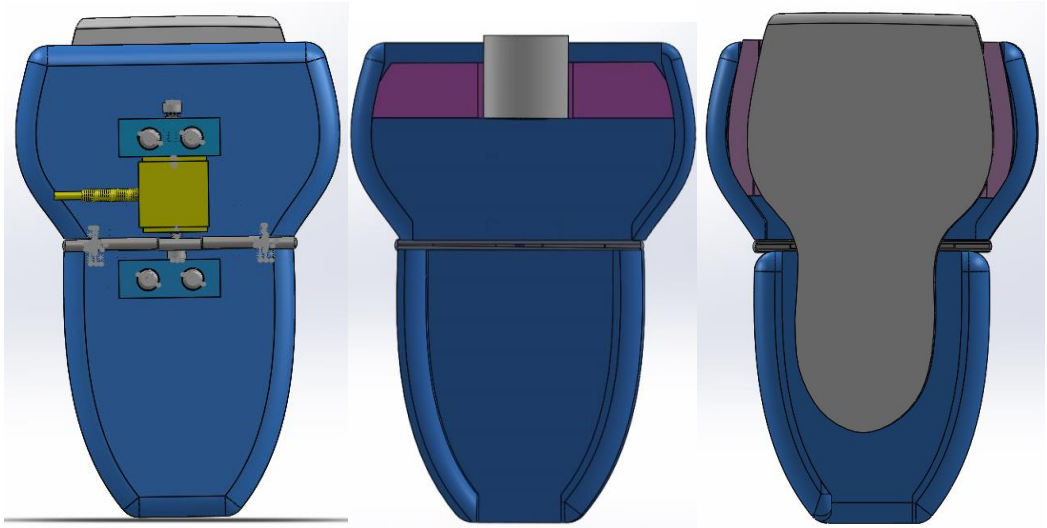

**(a)** **(b)** **(c)**

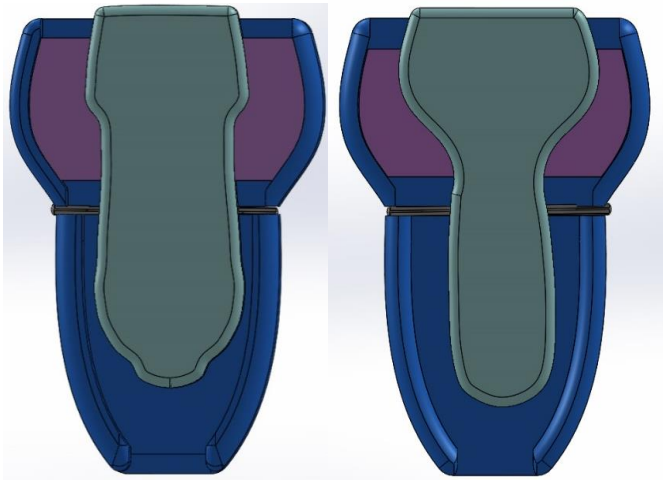

**(d)** **(e)**

**Figure 4.4: ultrasound transducer holder final design**


**Figure 4.5: prototyped transducer holder for different probes**

## Section 4.1.2: Component Design and Selection

This section presents the hardware used to help the user to control the device, with a description of each component. A miniature S-beam load cell from Futek Advanced Sensor Technology is used to measure the force between the ultrasound transducer and the device shown in Figure 4.6.


**Figure 4.6: LSB200, 5lb, JR S-Beam sensor. Dimensions: 0.27*0.75*0.69 (in) (http://www.futek.com/product.aspx?t=load)**

A very lightweight (9 gr) JR S-beam load cell with shunt calibration with 6.86x19.05x17.53 mm dimension has been used. There are different types of calibration, each of which gives the sensor different range and sensitivity. We prefer to choose shunt calibration with the bridge resistance of 351 Ohms and shunt resistance of 4mV/V and therefore the output of 21700 Ohms. The S-beam Futek load cell output voltage is proportional to force but calibration has to be programmed. An Arduino program collects these voltages. Each voltage has a range of -0.0006 to 1.8985mV/V. So, the program converts this voltage to data with units of pounds and Newtons using the calibration information described in Appendix B.

The system first reads the load cell data from an LSB200, 5lb, JR S-Beam sensor from Futek Advanced Sensor Technology. The load cell used in this project can tolerate an applied force up to 5 lbs with 1000% of R.O. safe overload. A breadboard circuit (Figure 4.7) uses an operational amplifier (op-amp, LM324) to process the signal.

However, the results recorded from the load cell were not accurate and the load cell exhibited a lot of noise. So, an ADS1115 16-bit analog-to-digital convertor (ADC) with programmable gain amplifier [33] has been used to compensate for this.

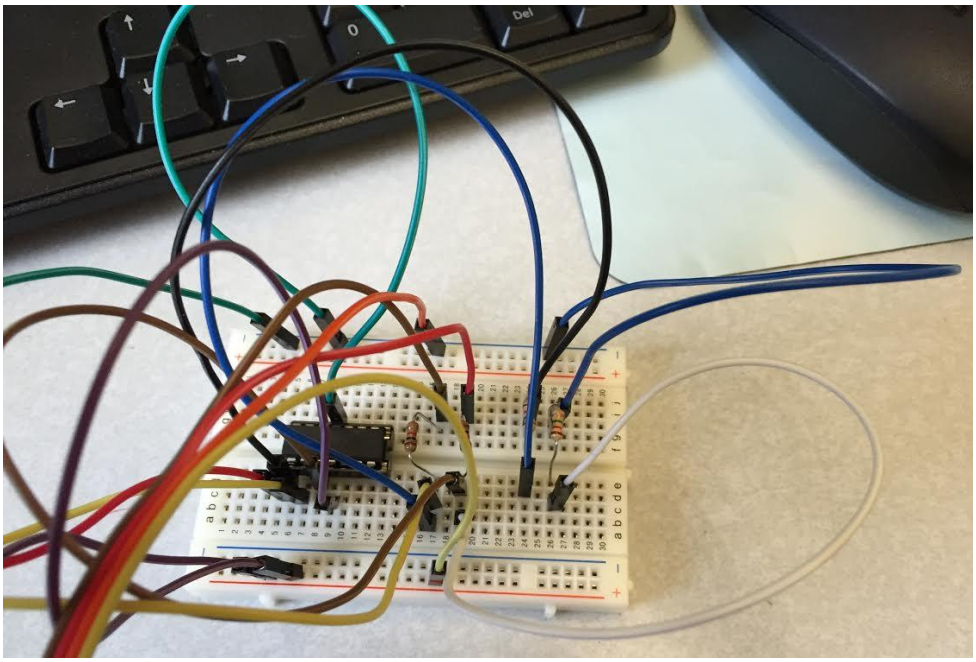

**Figure 4.7: The first designed load cell circuit**

This recorded force is an amplified measure of the force that has been applied to the patient's body by an operator's hand, based on the lever arm of the hinge and the relative placement of the load cell (Figure 4.3). The load cell is mounted on the back of the device between a plate and a hinge attached with two stainless steel socket head cap screws, which prevents the moment from being transferred to the probe along the axis of the hinge. The user holds the device and places it on the patient's skin. A 3-axis accelerometer (ADX335) is used to give a precise orientation of the device to the user. A

LCD is used to show the changes of applied force to the patient's body and the data from orientation of the device to the user. An orientation sensor must be used to measure the gravity vector and the relative angle of the transducer holder axis. Since the output voltage from the load cell is very small (0 - 7.8 mV), and the raw signal to noise ratio is poor, we need to design a circuit to get data from the load cell when the force is applied. So, an operational amplifier (op-amp, LM324) shown in Figure 4.8 [34] has been used with a differential amplifier circuit shown in Figure 4.9 [35] for amplification of the results obtained from the load cell using a board with two resistors of 1000 Ω and two of 1MΩ in order to add the two analog signals. By changing the values of two resistors $R_1$ and $R_2$, we can change the values of the output recorded from the load cell. To simplify the board, we chose the same resistors for $R_1$ and $R_2$ so that $R_3$ and $R_4$ are equal. The equation used for the output voltage signal based on the input signals and the values of the four resistors from [36] is:

$$Vout = -v1\left(\frac{R3}{R1}\right) + v2\left(\frac{R4}{R2+R4}\right)\left(\frac{R1+R3}{R1}\right) \qquad \textit{eq. 4.1}$$

In this circuit the resistor used for $R_1$ and $R_2$ is 1kΩ and $R_3$ and $R_4$ is 1MΩ. The op amp used in this circuit amplifies and inverts the output voltages, and the data for the output voltage will be between -5V and +5V.

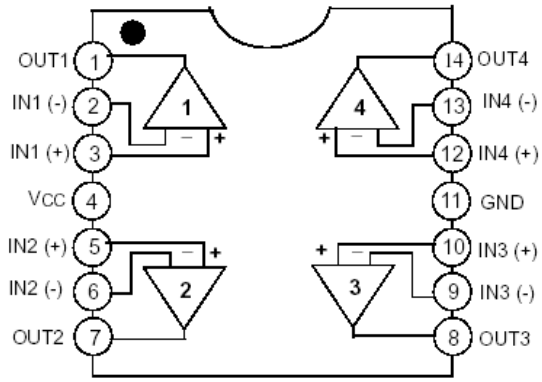


**Figure 4.8: LM324 – Quad Op-Amp, (http://www.epanorama.net/cgi-bin/semi.cgi?keyword=LM324)**

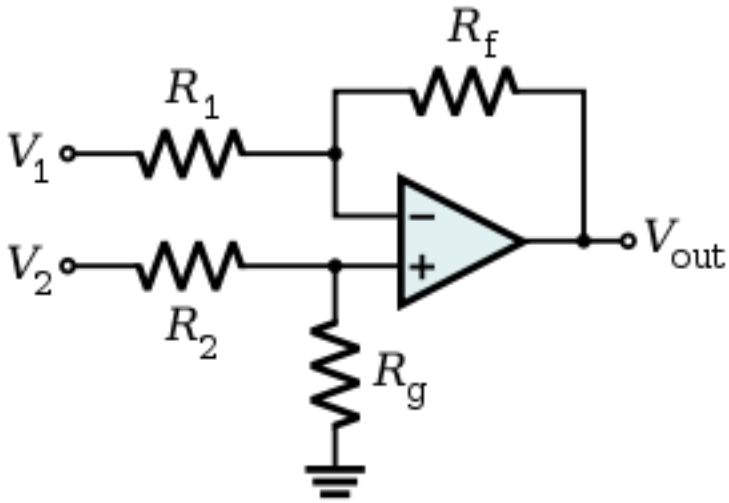


**Figure 4.9: Circuit Diagram, (https://en.wikipedia.org/wiki/Differential_amplifier)**

The signal from the load cell was imprecise because the Arduino Mega has 10 bits of resolution and because the voltages read from the load cell are relatively small with respect to this resolution. So another circuit design has been used to get more accurate data. For this design an ADXL335 16-bit 4-channel ADC with programmable gain amplifier [37] has been used. The circuit is shown in Figure 4.10. Equation 4.2 has been

used to determine the ADC resolution. $V_D$ is the input voltage range (5V for this system) $V_S$ is the output voltage range of the signal, which is 20mV, *n* is the bit resolution of the ADC, which is 16 bits according to the ADC used in this system, *B*, the bipolar range, is 1, and *E* shows what $V_S$ represents the full-scale output voltage range of the signal we want to measure, which is 5lbs for the load cell used in this project.

$$\text{Resolution} = (V_D \times E)/(V_S \times 2^{n-B}) = 0.038 \text{ lb} = 0.169 \text{ N} \qquad \textit{eq. 4.2}$$

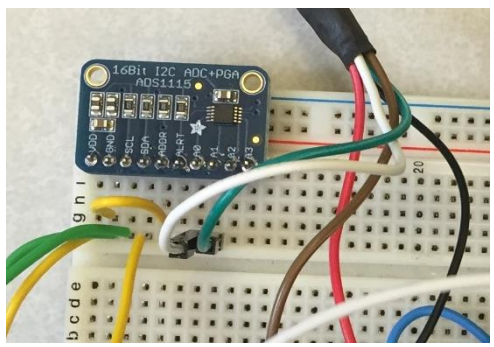


**Figure 4.10: ADXL335 circuit**

The final system setup includes parts purchased from Adafruit, Futek, and McMaster-Carr. Table 4.2 lists the components with the manufacturer's descriptions. A picture of the hardware setup of the design is shown in Figure 4.11. Figure 4.14 shows the breadboard circuit of components used to control the device. Also, Figure 4.13 shows the coordinates of the device, ultrasound transducer, and load cell. Also, a female DC power adapter - 2.1mm jack to screw terminal block has been used to prevent damaging the Arduino board for powering up too many items through one board. Therefore, the

LCD display is powered up through this DC power adaptor. Figure 4.13 shows the range of motion of the device when the force applied to the body.

**Table 4.2: Components used for controlling the device**

| | |
|---|---|
| 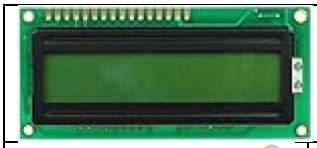 | Standard LCD 16x2 LCD Display |
|   | FlexiForce A201 Sensor |
|   | LSB200, 5 lb, JR S-Beam Load Cell |
|   | Arduino MEGA 2560 |
|   | ADXL335 - 5V ready triple-axis accelerometer |

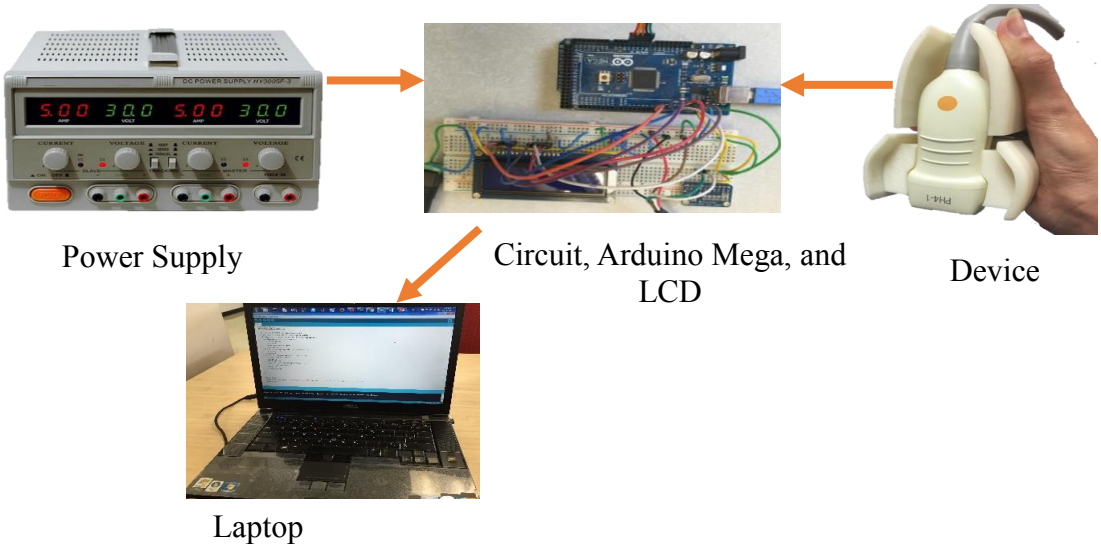


**Figure 4.11: Hardware used for measuring applied force**

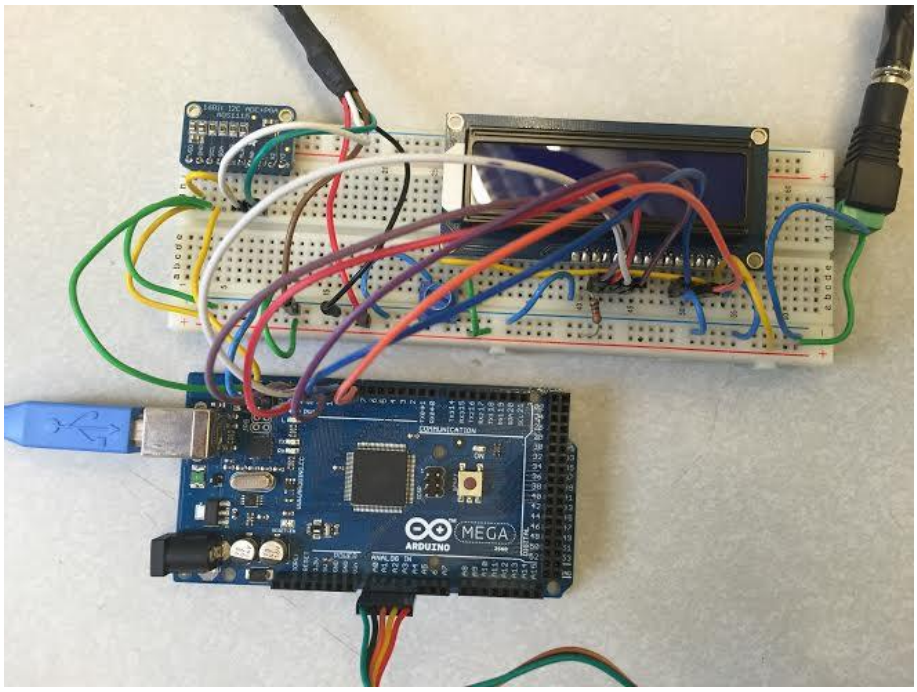


**Figure 4.12: Components used for controlling the device**

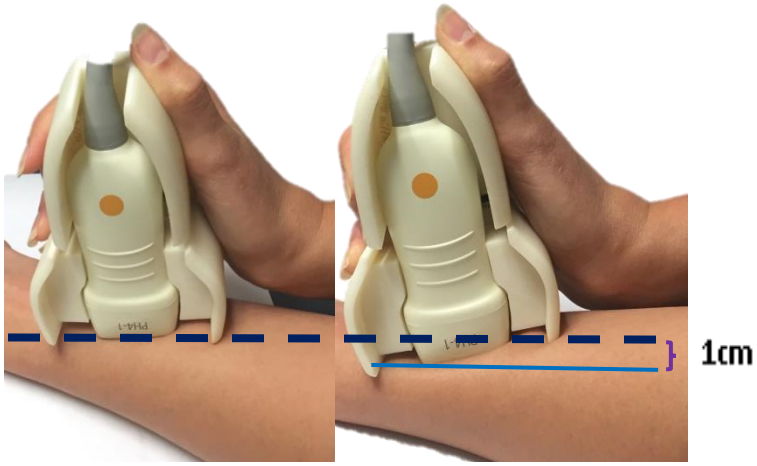


**Figure 4.13: Range of motion of the device by applying Force**

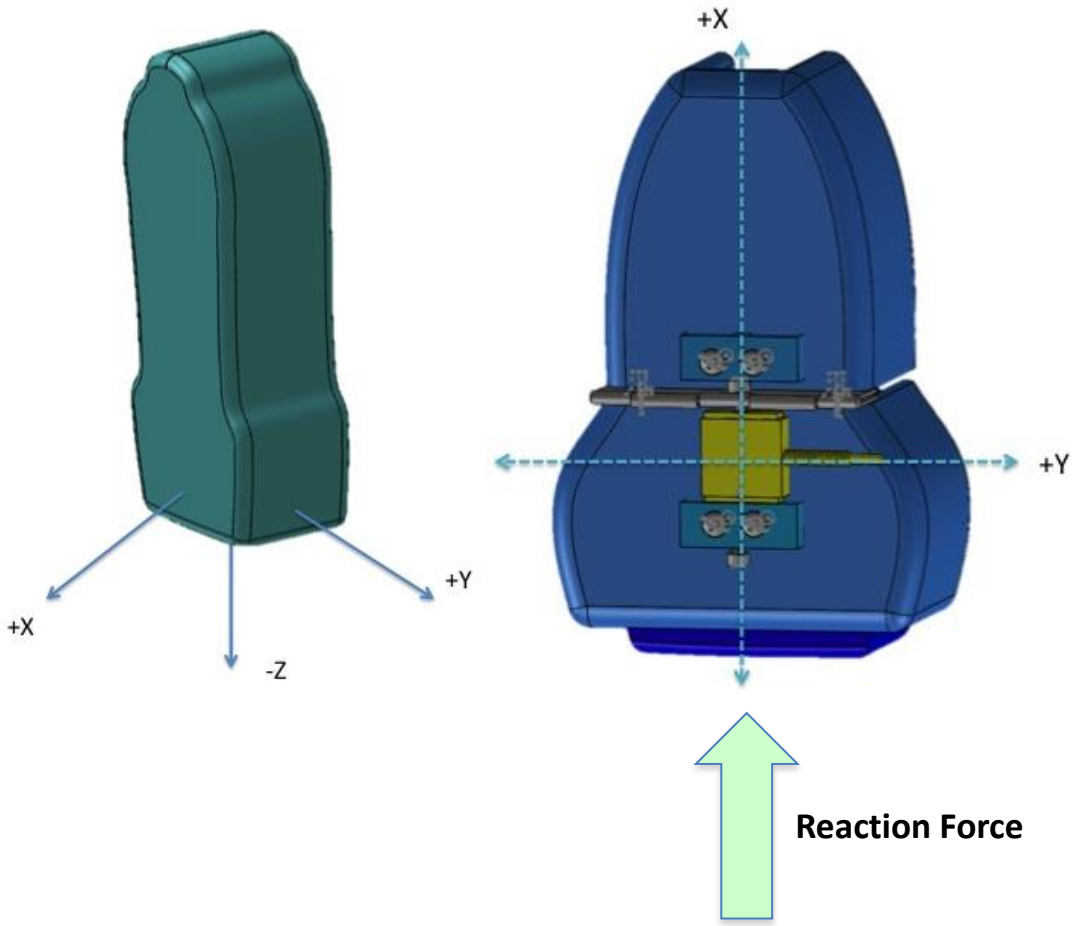


**Figure 4.14: Coordinate diagram of transducer (left), coordinated diagram of load cell (right)**

As a summary of this section, Figure 4.15 shows interactions of the information in the system between different components. Future work is needed to make the device smaller to be held by the user's hand more comfortably. The next part illustrates the design of the device to control the position and orientation of the ultrasound transducer. The system uses an accelerometer installed on top of the device.

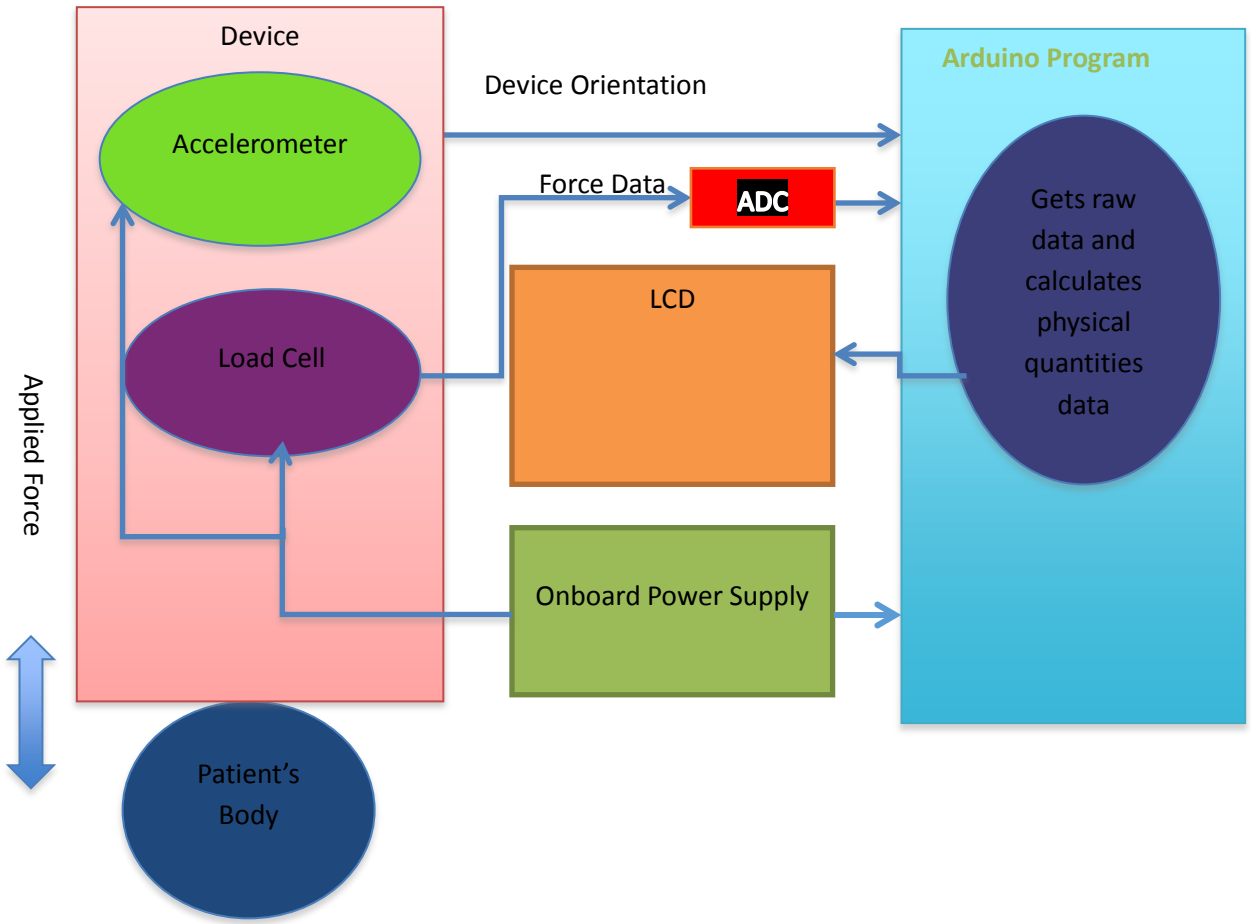


**Figure 4.15: Interacting information into the system**

# 4.2: Orientation Display

To measure orientation of the device, a 3-axis accelerometer, ADX335, shown in Figure 4.16 has been used. One 16x2 cell LCD display has been used to show the data from movement of the device and changes of orientation of the device when the device is held by the user. Some research has been done to create a way to generate 3D images where a position tracking system has been used to record the movements of the user's hand [38]. In real ultrasound applications, the user does some linear or rotational motions for imaging a particular area in the body.


**Figure 4.16: ADX335 Accelerometer, (http://www.adafruit.com/product/163)**

## *4.2.1: Hardware Components and Circuit Design Selection*

In the experiment a small force will be applied to a phantom made out of silicone Ecoflex 20 measured with a load cell, and some unskilled subjects will test the device to see if force accuracy improves. A Siemens Antares system equipped with an Axius Ultrasound Research interface has been used for one experiment. The transducer's transmit frequency is set to 5 MHz. The data from ultrasound frequency are recorded. For

using the device to measure applied force in a very small part of the body such as measuring blood flow after intracranial pressure, a 2MHz transducer, Doppler X by DWX Compumedics is been used that is a very tiny probe for small applications. Also, three different phased array probes have been used (the VF 7-3, the PH 4-1, and the VF 13-5, all manufactured by Siemens). Fifteen subjects have been chosen to use a phantom made out of silicone instead of using human subjects.

## *Section 4.3: Software and Integration*

An Arduino program is used for displaying the force applied to the body and the orientation the probe. This program collects the force data applied to the patient's body. Then it will send digital voltage data to an LCD according to that recorded force. In experiments, a small LCD was used. The interface of the small LCD display has been divided in two sections: the top section for representing the data from the accelerometer to show the transducer holder axis in degrees, and the bottom section for showing the load cell data from measuring applied force to the patient's body in a bar format. Figure 4.17 shows the whole control system with the prototyped setup of the device.

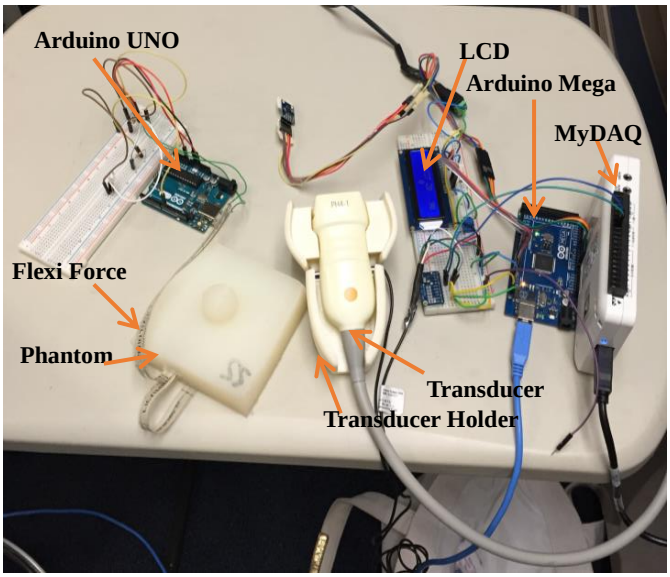


**Figure 4.17: The whole system setup ready for doing experiments**

For the convenience of the user, a large color LCD display was used to observe the results of orientation and load cell on a big screen. A large touchscreen LCD (Figure 4.18) is used to create intuitive graphics for the users. Images, large readouts, and the use of color will enable users to receive quick feedback as they perform training protocols using the device. Future work is needed to test the device using the touchscreen LCD and getting feedback from the operators. A digital readout of the force is coupled with a 'power bar' display that has the target amount of force in yellow, with the color red indicating too much force and green indicating that more force is necessary. Digital dials are used to displace the transducer's orientation.

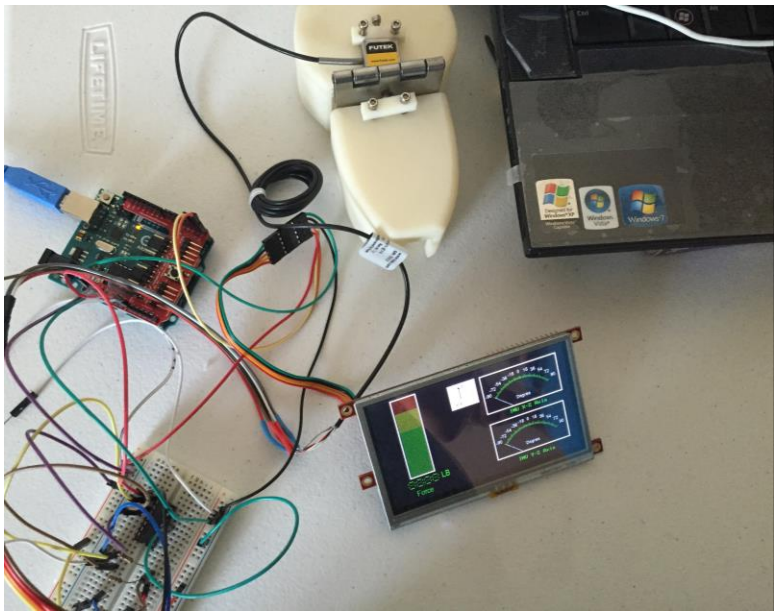


**Figure 4.18: Initial circuit integration on load cell and IMU with breadboard and touchscreen LCD**

# Chapter 5: Results

This chapter describes the results of several experiments to evaluate the performance of the device. We first investigated the load cell calibration of the device, and then used the device to test the efficacy of the device in ultrasound training purposes. We also compared the ability of our system to facilitate the application of sustained constant contact force by untrained operators.

## *Section 5.1: Device Testing/Evaluation*

The next step was testing the device by ten different researchers. The user holds the device and puts the device in contact with the phantom. The input of the system would be the motion of the user's hand and the outputs are the measured force and orientation of the device. Figure 5.1 represents this interaction.

The first step of testing the device was investigating the ability of the device to achieve a target contact force. The phantom used in the experiments (made out of Ecoflex 20) had similar mechanical properties of skin and soft tissue. The device holding the ultrasound probe was placed in contact with the phantom, applied force on the phantom is 4.22 N.

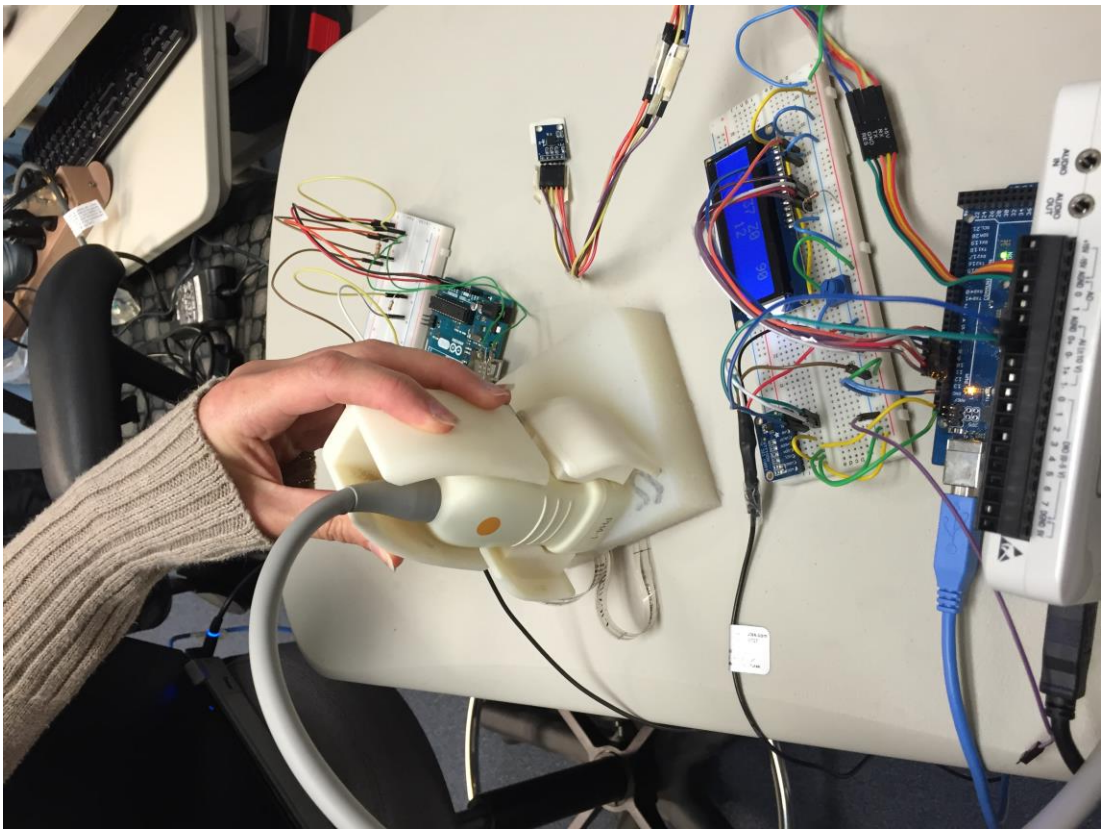

**Figure 5.1: The device held by user's hand, applying force to the phantom**

An embedded FlexiForce A201 force sensor [39] was used to measure force near the vessel cavity in the silicone phantom. A single-element ultrasound transducer was mounted directly to a load cell to measure the applied force. Figure 5.2 shows the FlexiForce circuit and the diagram from [40] used for that circuit. Figure 5.3 shows the hardware used to control the device.

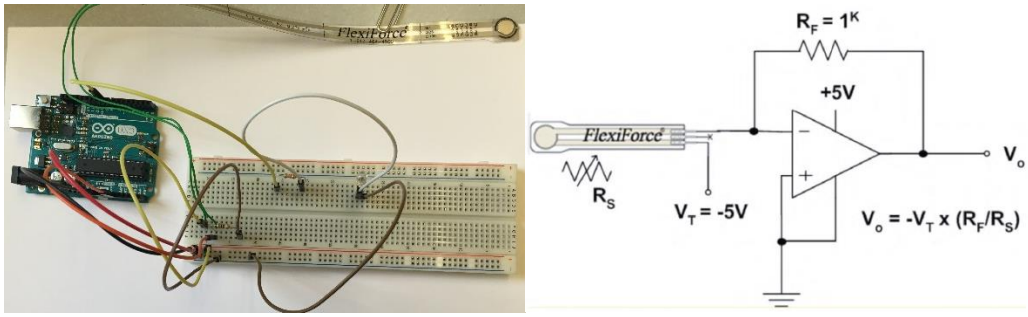


**Figure 5.2: left: FlexiForce circuit, right: FlexiForce diagram**

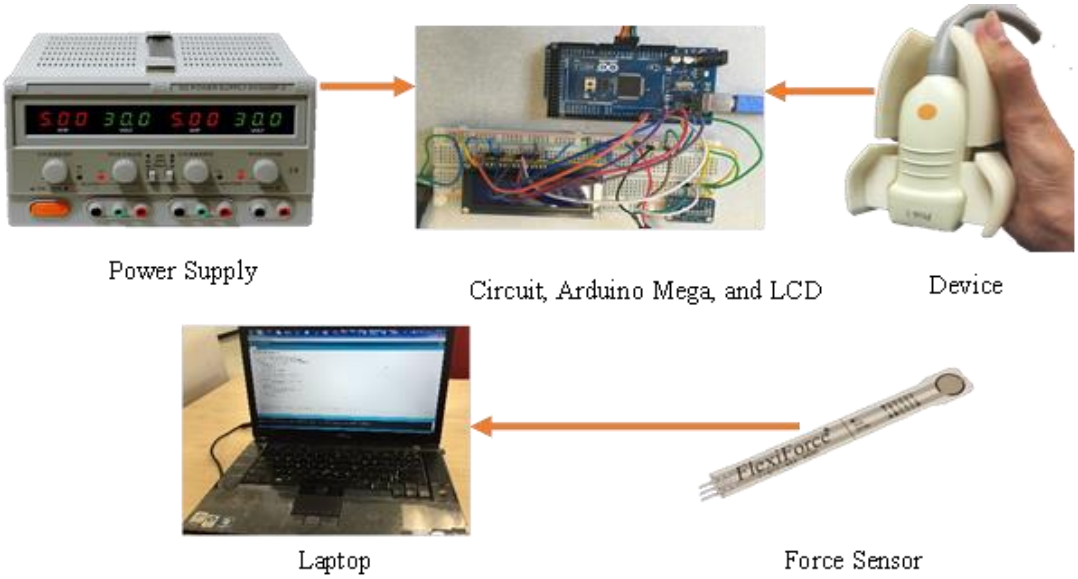


**Figure 5.3: Hardware used for measuring applied force**

The user holds the system with his/her hand and then puts the system in contact with the phantom surface, applying forces to the phantom. A Flexiforce sensor located in the middle of the phantom (1cm below the surface of the phantom) shows the applied force to the phantom through a laptop monitor. The data from Flexiforce sensor captured from monitor of a laptop using an Arduino program to record measured received force through the phantom. This chapter illustrates the results from different experiments using the device. Experiments have been done using 10 different users to test the device using and not using real-time visual feedback using a MyDAQ system using a LabVIEW program to record the data from subjects testing the device to get the device efficacy.

We also tested the device to get the accuracy of the force and orientation system using an ultrasound machine. Figure 5.4 shows the images recorded from the ultrasound

machine when the device was used to image carotid artery. Typical ultrasound examinations of the carotid artery require contact force of up to [40]. In this test, 6 N of force was applied to the carotid artery and measured from the device and shown into the LCD. This test demonstrated that good quality images can be acquired using visual feedback of applied force. Red color in the right image shows the blood flow running through the probe and blue shows blood flow going far from the probe. Having this force information as well as information on probe orientation is assumed to help unskilled individuals obtain these types of images; further testing is needed to prove to what extent this is an improvement over imaging by unskilled individuals without feedback.

Figure 5.5 shows the mini transducer held by the device tested on a simulated eye to the phantom to show the possibility of testing the device on mini transducer to the eye in future testing.

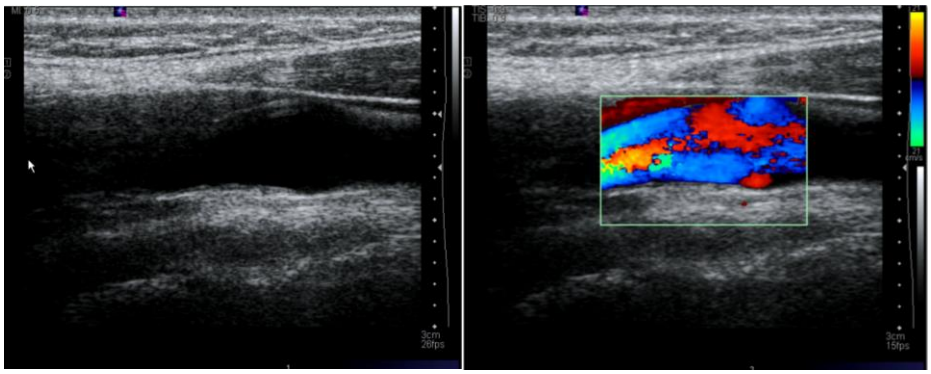

**Figure 5.4: Recorded photos from ultrasound machine using the. black and white carotid artery (left), color carotid artery (right)**

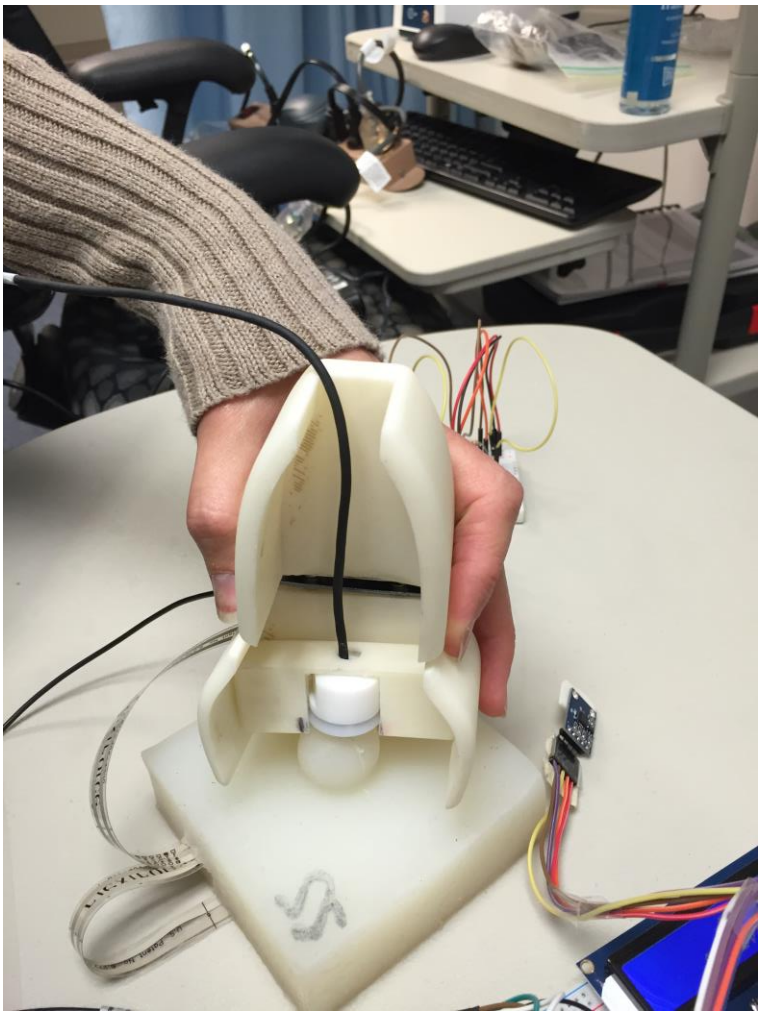

**Figure 5.5: Mini transducer tested on a phantom**

Before doing the actual experiments using human subjects to figure out what the scaling factor is between the value read into the Arduino from the ADC and the actual force, a known load was directly applied to the load cell and the signal on the serial monitor was observed. The appropriate conversion factor was then applied so that the LCD displays the value of force in N. For doing this calibration, a two-part jig was designed in SolidWorks and then made using a laser-cutting machine. Figure 5.6 shows the steps of getting the scaling factor of the load cell.


**Fig. 5.6: load cell calibration, laser cut part to do calibration (top), applied 1/2lb force (bottom left), 3lb (bottom right)**

We tested the device to get information about the ability of the system to achieve a target contact force. Users have been asked to test the device by holding it and applying a target force on the phantom with and without the LCD feedback to see if force accuracy improves. The experiments have been done using 10 unskilled users. Some information was provided to the users as a familiarization session so that the users understood how to use the device. Each user tested the device in three trials each with and without the LCD feedback. Three lbs of force was applied to the phantom and the data from the load cell were recorded through MyDAQ using a LabVIEW program. After reaching the target

force, the applied force was held for 10 seconds. The same test was repeated with and without visual feedback for 3 trials of using and not using the LCD for each user. The following graphs show the resulting force data.

The first user was an untrained person using the device for the first time. After familiarization about the concepts of the device and steps of performing the demonstration, the data recorded until the subject reached the target force (3 lbs or 13.345 N) using LCD for having a real-time visual feedback. The user continued applying force to the phantom for 10 seconds, and then stopped. The test was repeated three times with and without having visual feedback from LCD and 6 times in total. The following figures are showing the measured force from the load cell mounted on the device. The target force is shown as a blue dashed line. Figure 5.7 shows three repeated tests with visual feedback. The same three graphs are compared together to analyze if repeating using this device with having visual real time feedback improves ultrasound-training performance. The graph shows that after using the device once, the second and third tries have improved and the subject could reach the target force faster. Figure 5.8 shows three tries of using the device without using the LCD and Figure 5.9 compares with and without having feedback in one graph to see the differences.

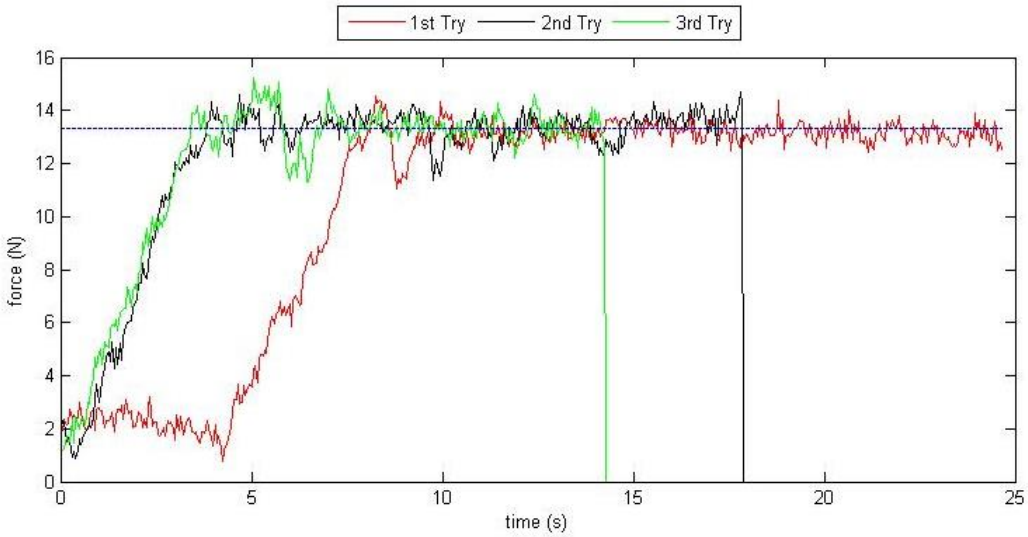


**Fig. 5.7: 1st subject testing the device repeated three times with having visual feedback**

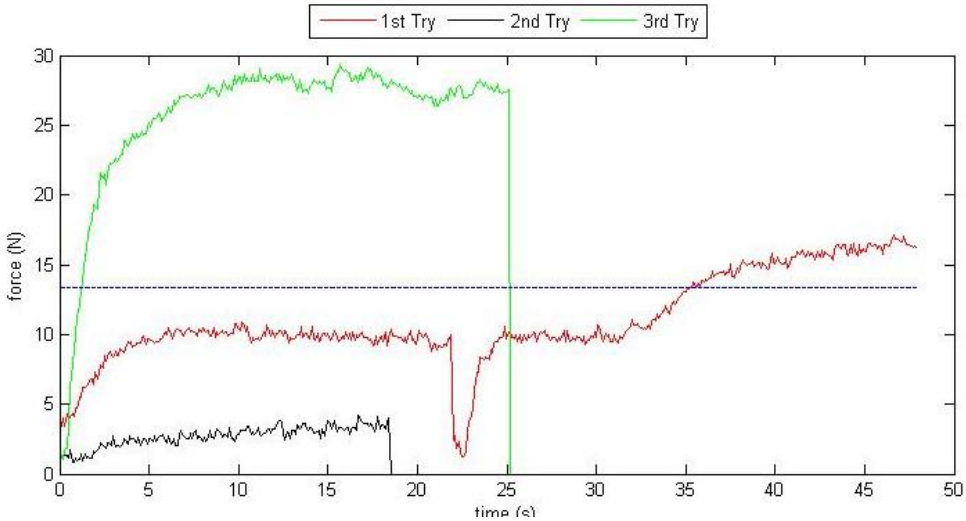


**Fig. 5.8: 1st subject testing the device three times without using LCD**

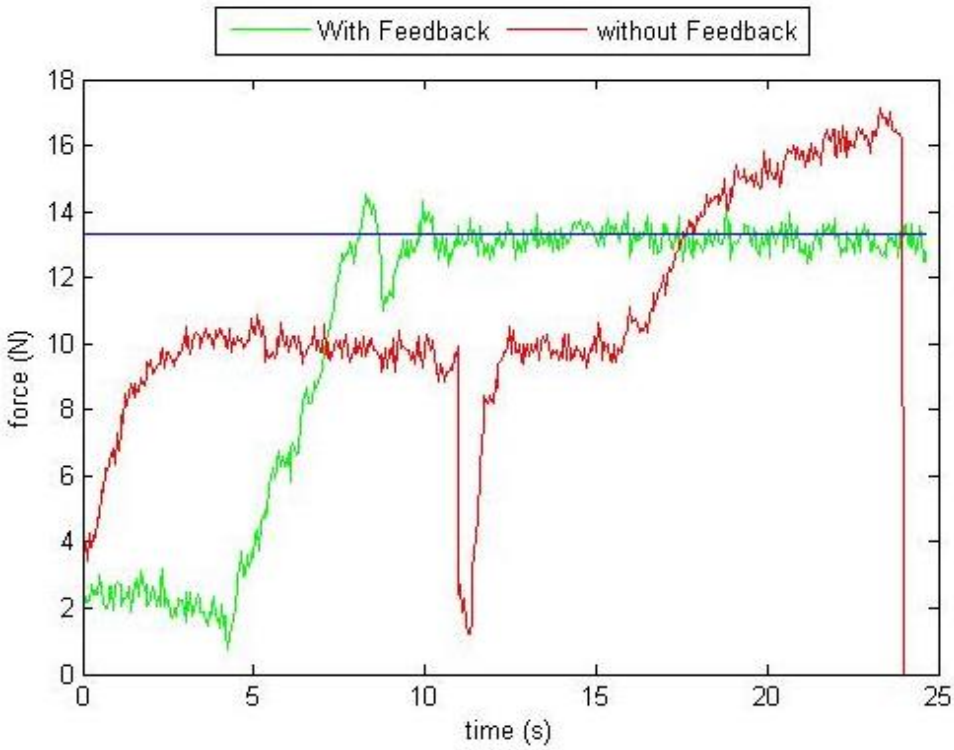


**Fig. 5.9: 1st subject with and without feedback for the first try**

The next figures are the analyzed data recorded from the second untrained user. Figures 5.10 and 5.11show that this user, without the aid of LCD feedback, misjudged the target force but held relatively steady. Figure 5.12 compares one test using and not using the LCD.

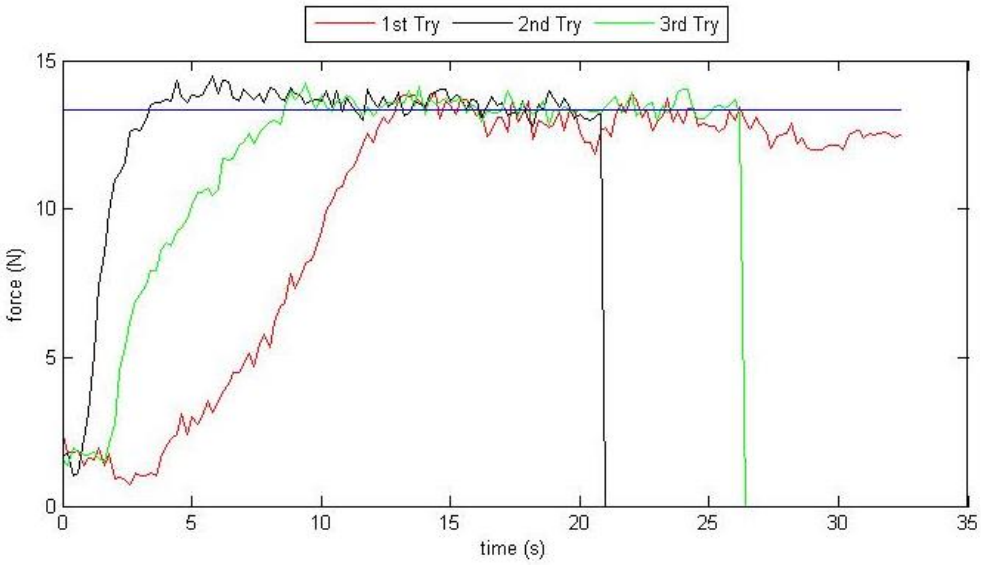


**Fig. 5.10: 2nd subject using visual feedback**

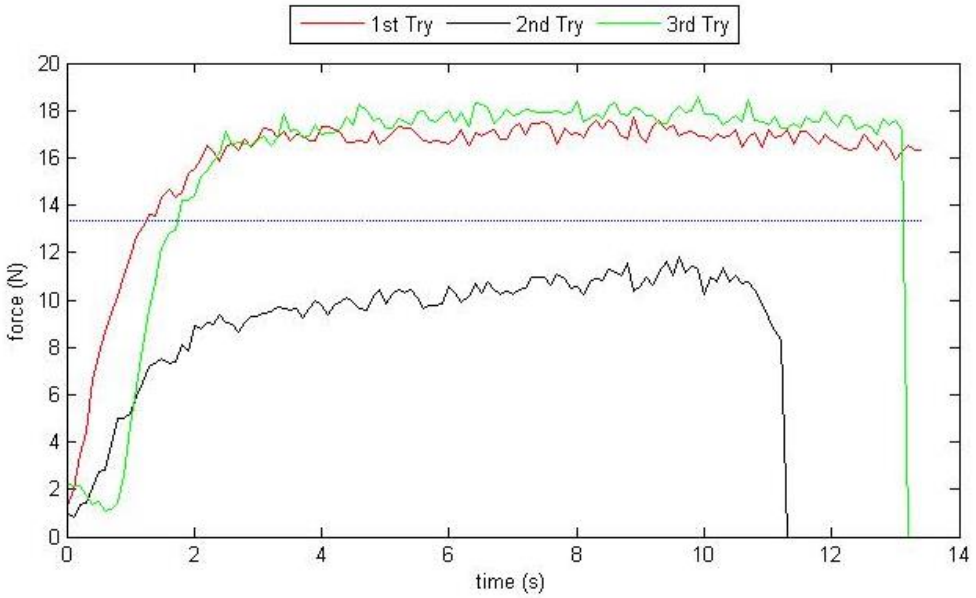


**Fig. 5.11: 2nd subject not using visual feedback**

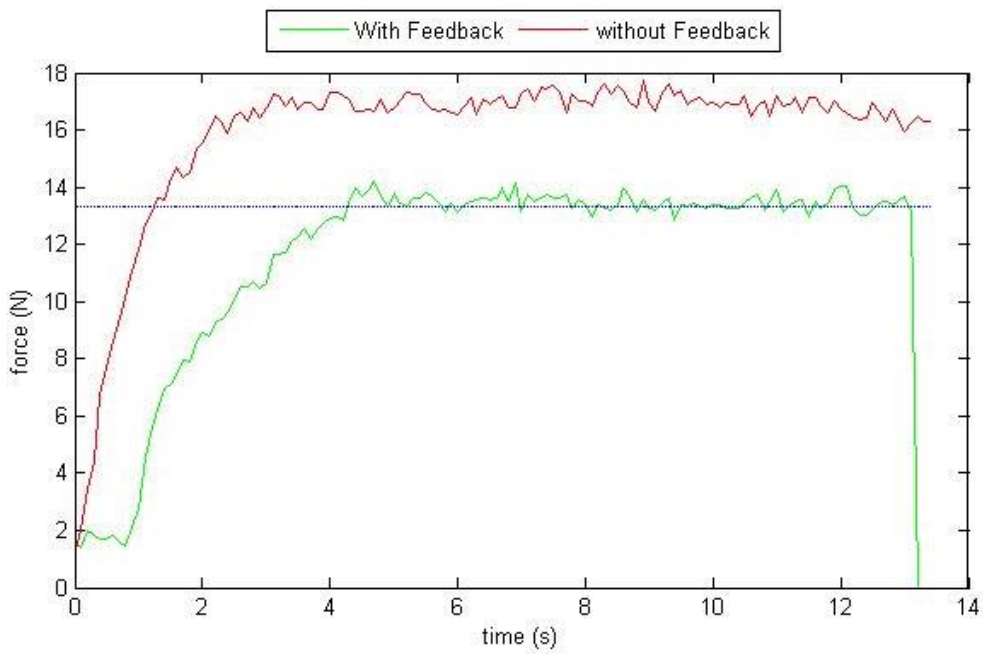


**Fig. 5.12: 2nd with and without feedback**

The third user was reaching the target force faster than others. Also, the recorded data shows that after sensing the target force with having a visual feedback, the user found it was easier to get close to the target force without having LCD feedback. Figure 5.13 shows three times of using the device with feedback from the LCD and Figure 5.14 shows three times without having feedback from the LCD. Also, Figure 5.15 compares a test of with and without visual feedback.

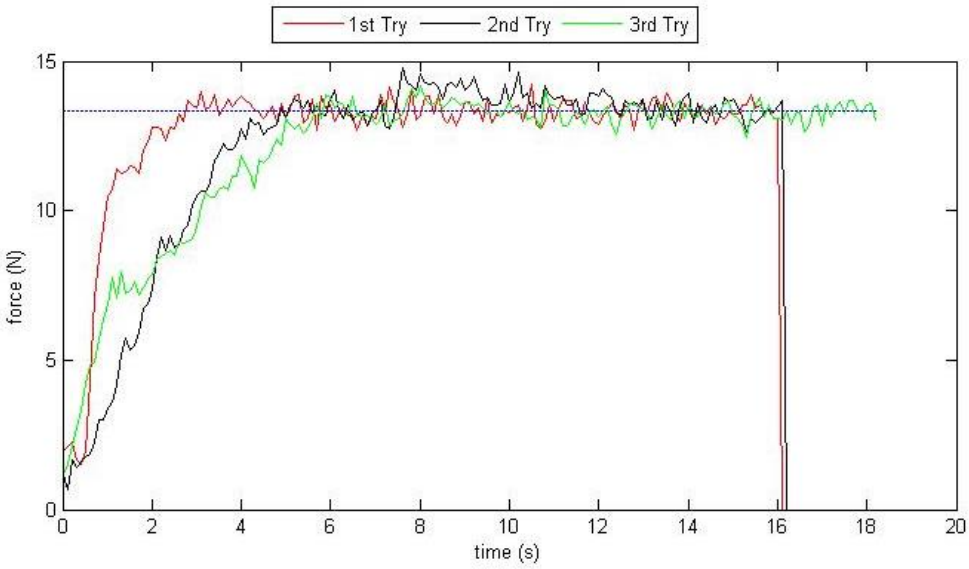


**Fig. 5.13: 3rd subject using visual feedback**

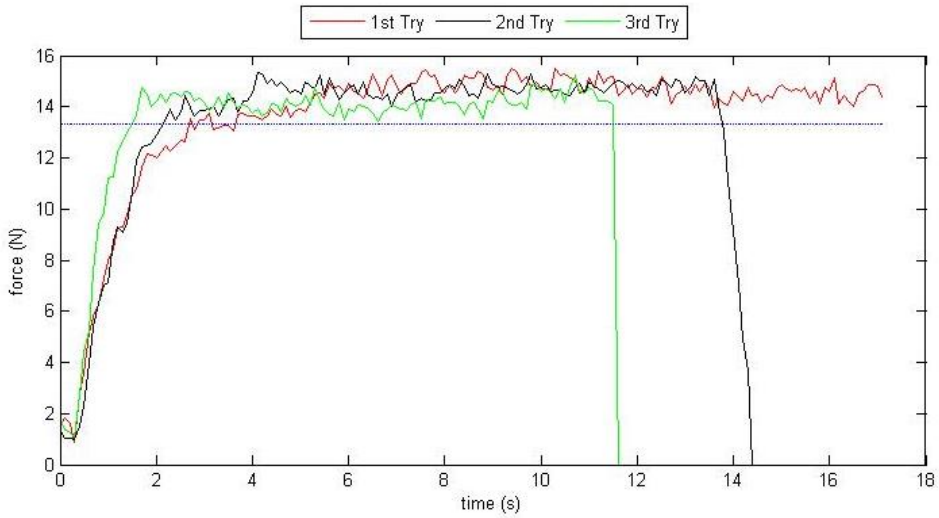


**Fig. 5.14: 3rd subject not using visual feedback**

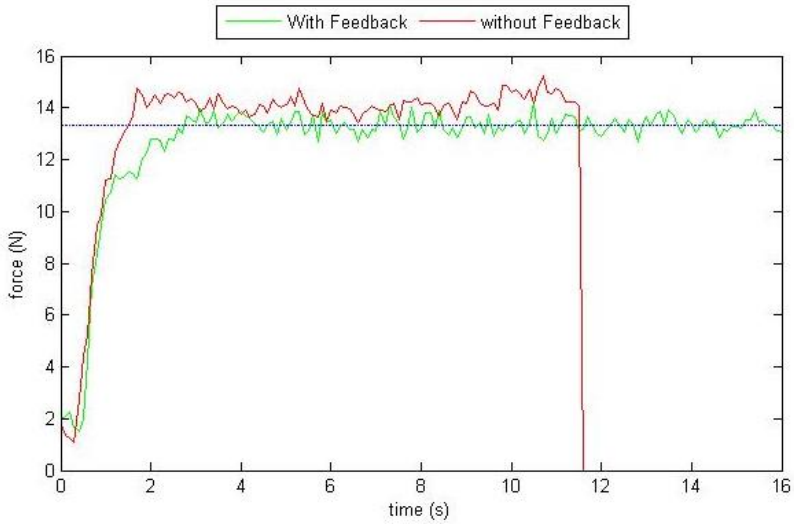


**Fig. 5.15: 3rd subject using and not using visual feedback**

The recorded data from the fourth user shows that it took 5 seconds for this person to reach the target force. Also, repeating the test just slightly improves the time taken to reach the target force compared to the first try. Figures 5.16, 5.17, and 5.18 present these differences.

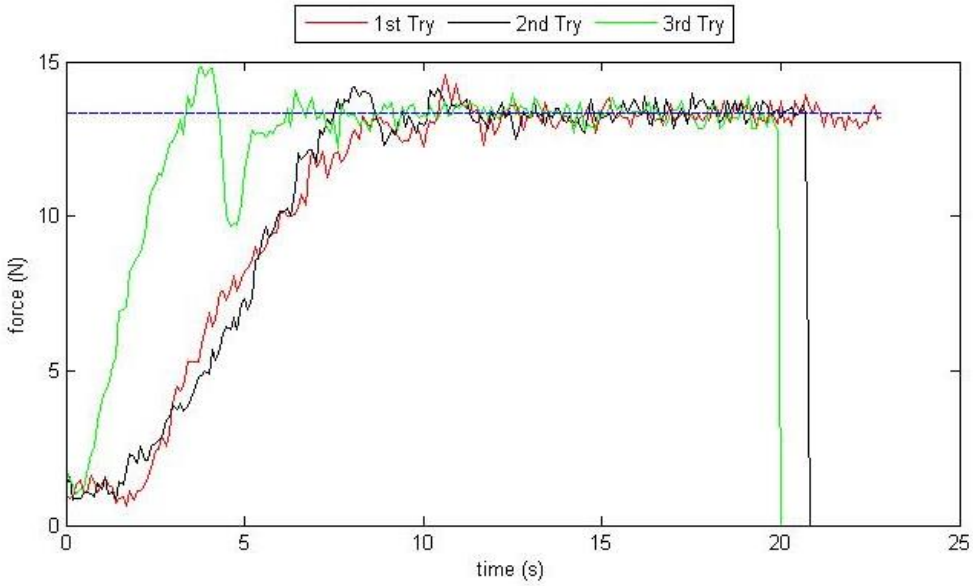


**Fig. 5.16: 4th subject using the device with having visual feedback**

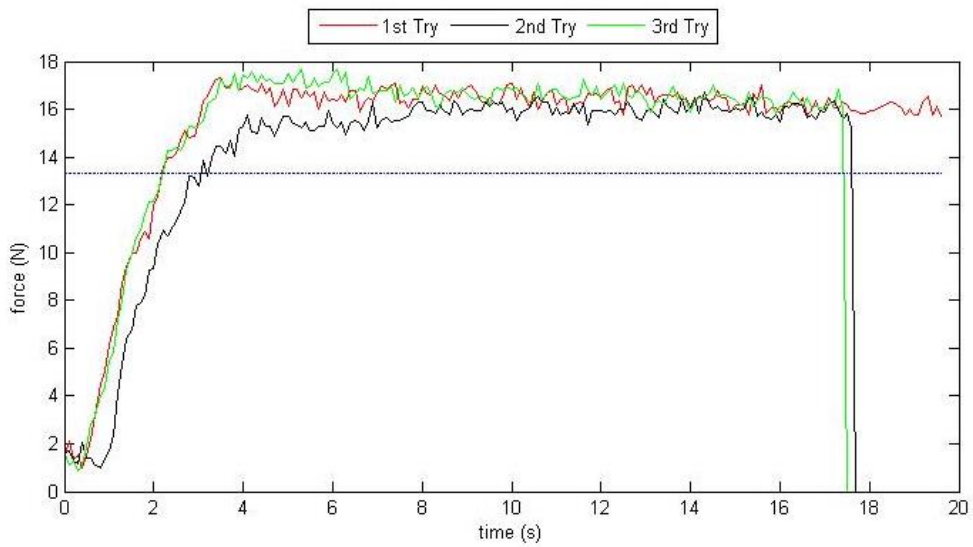


**Fig. 5.17: 4th subject testing the device without having visual feedback**

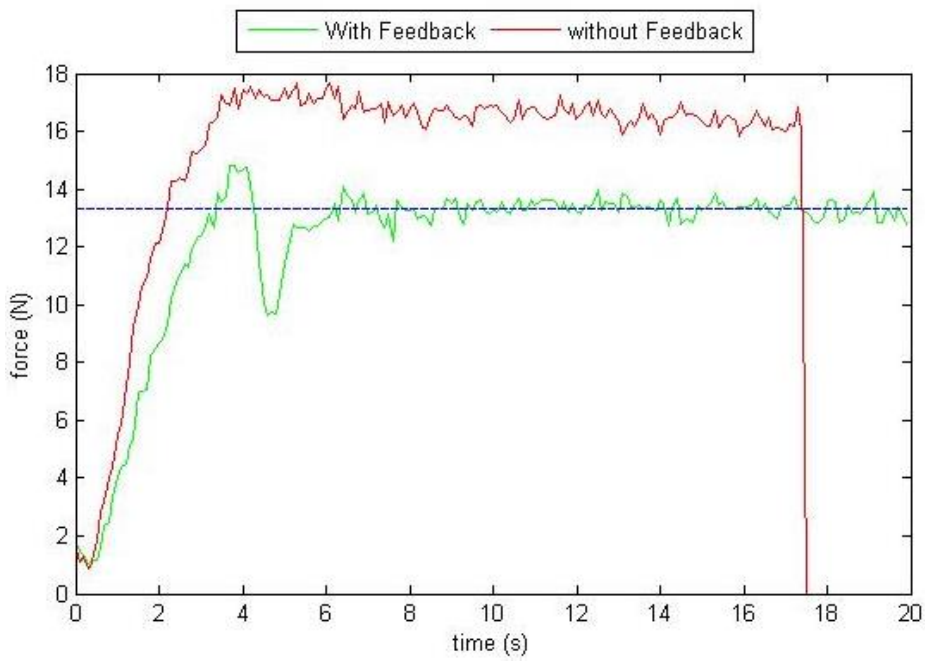


**Fig. 5.18: 4th subject comparing using and not using visual feedback**

The figures for the fifth user show that with real-time feedback the first try required about 20 seconds to reach the target force, but with repeating use, reaching the

target force got much faster (7 seconds) as shown in Figure 5.19. Also, after a couple times using visual feedback, reaching the desired force without having feedback became easier in the last try (Figure 5.20). Figure 5.21 shows the first try of with and without the visual feedback.

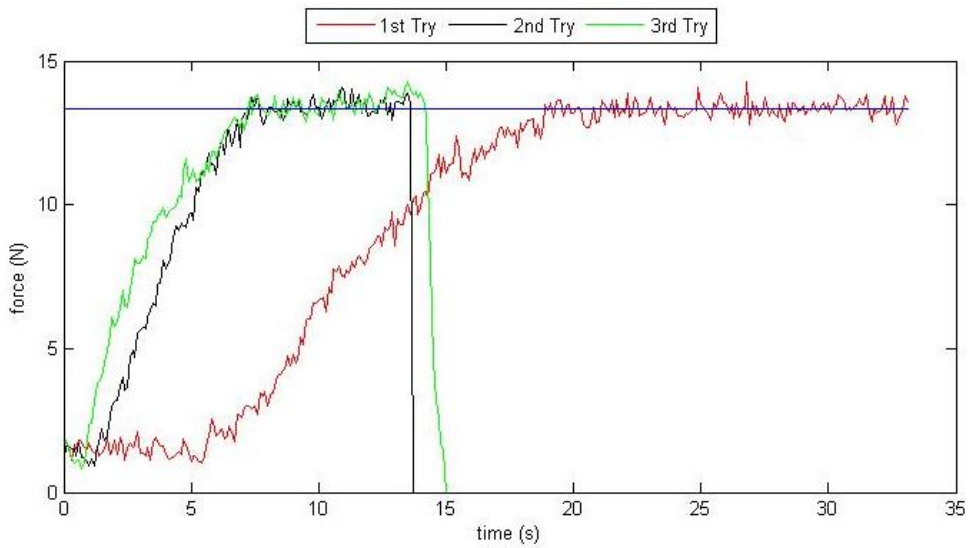


**Fig. 5.19: 5th subject using visual feedback in three tries**

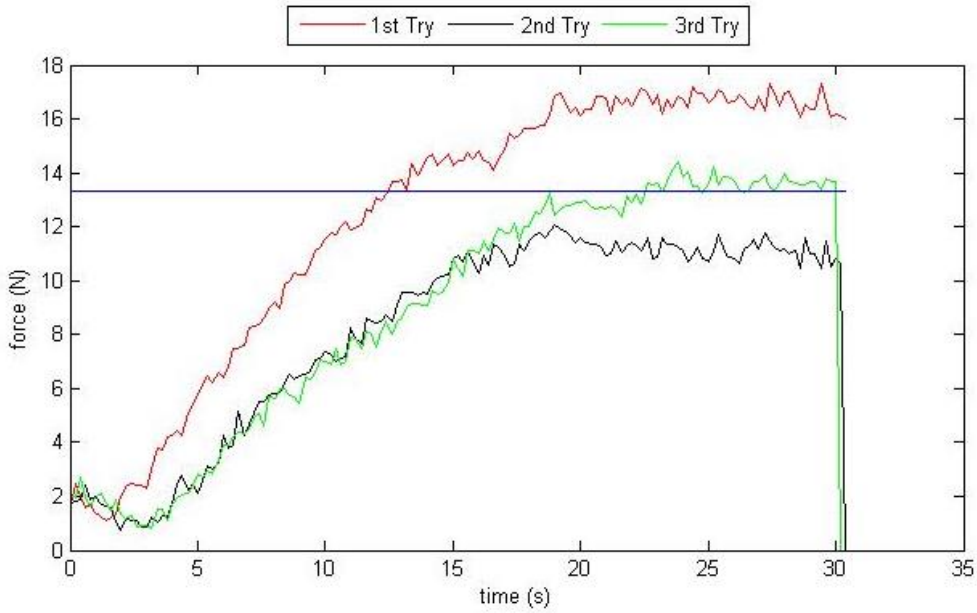


**Fig. 5.20: 5th subject not using visual feedback in three tries**

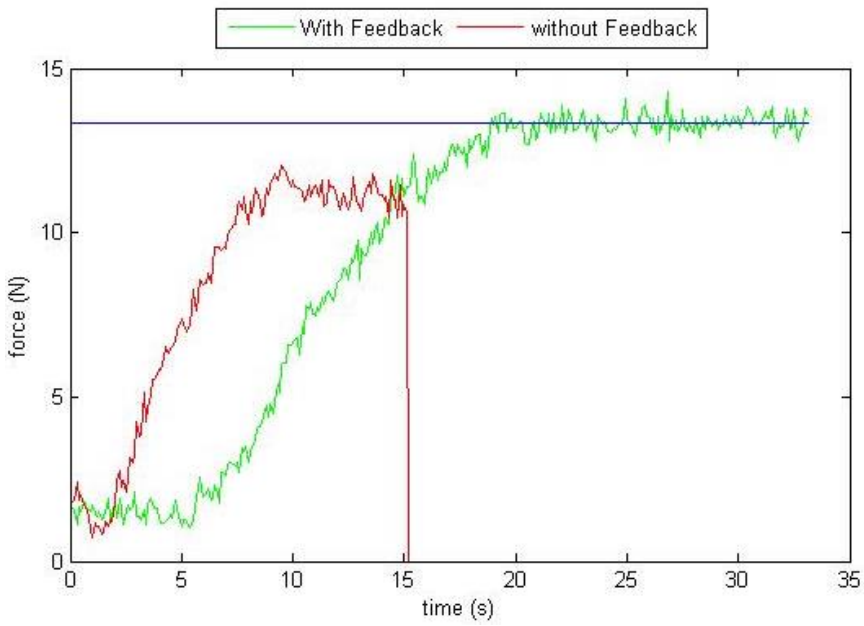


**Fig. 5.21: 5th subject using and not using visual feedback in first try**

The sixth user reached the target force after 5 seconds, and the data shows that the third try is better than the first two tries. This user performed pretty well even without the visual feedback. Figures 5.22-24 show these findings.

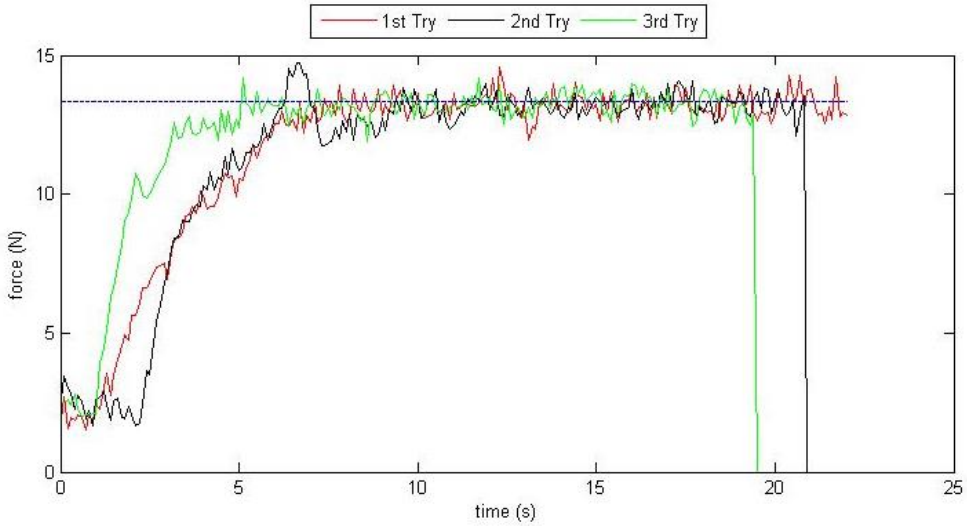


**Fig. 5.22: 6th subject using visual feedback in three tries**

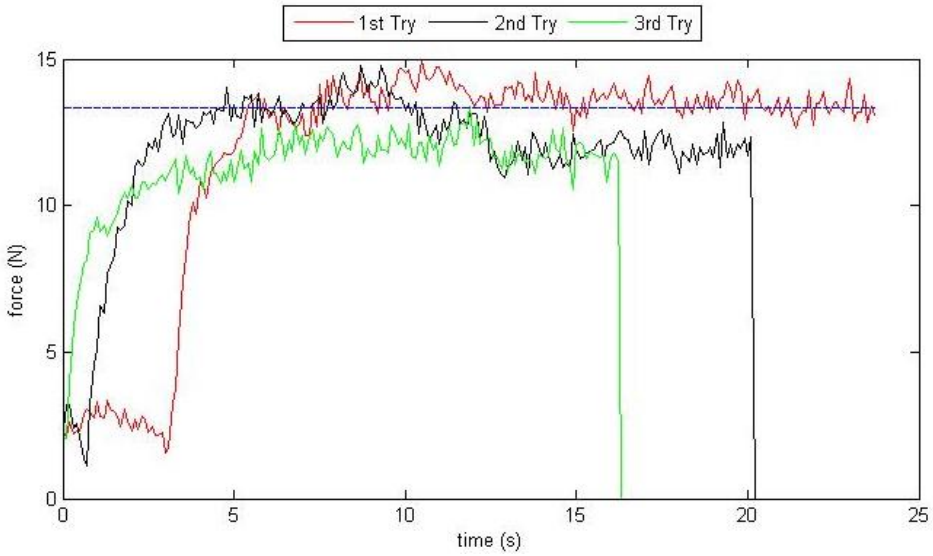


**Fig. 5.23: 6th subject not using visual feedback in three tries**

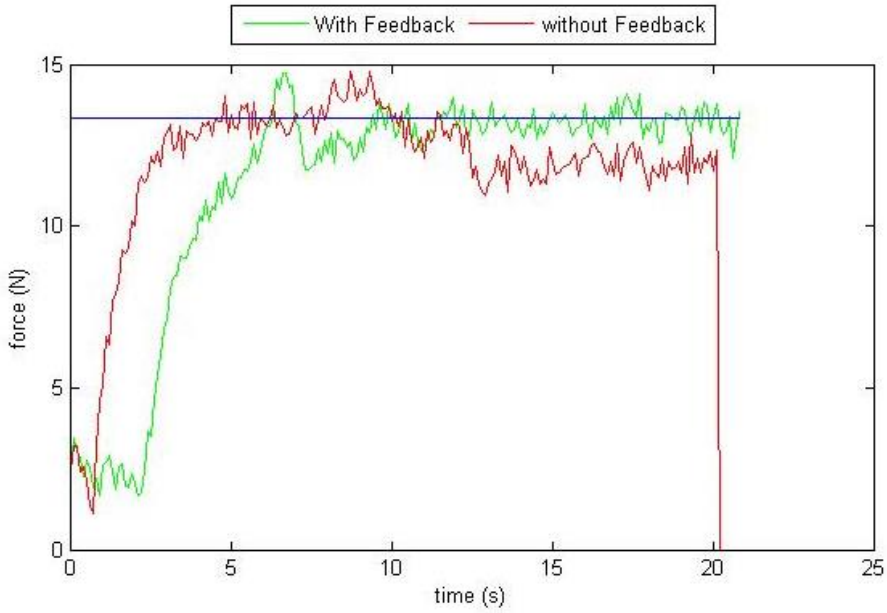


**Fig. 5.24: 6th subject using and not using visual feedback**

The measured data from the seventh user shows that at first it took a long time for this user to reach the target force. However, after three times of repeating this test, reaching the target force took less than 5 seconds, which shows the efficacy of this

device. Figures 5.25-27 show these results.

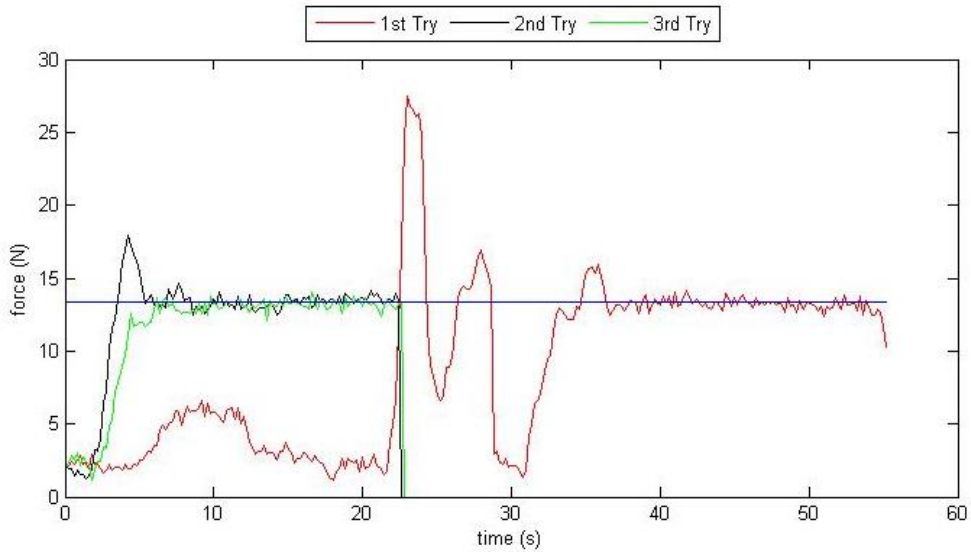


**Fig. 5.25: 7th subject using the visual feedback**

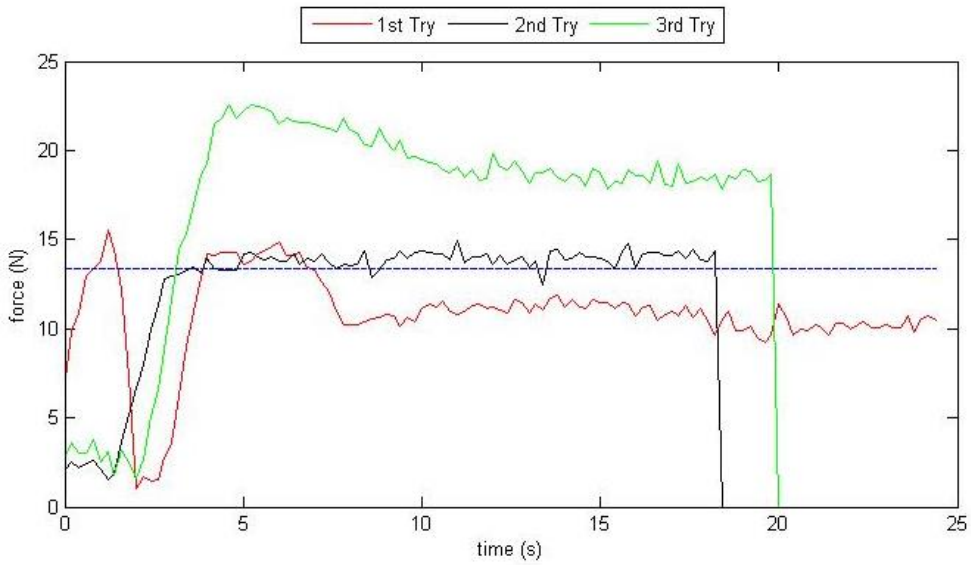


**Fig. 5.26: 7th subject not using visual feedback**

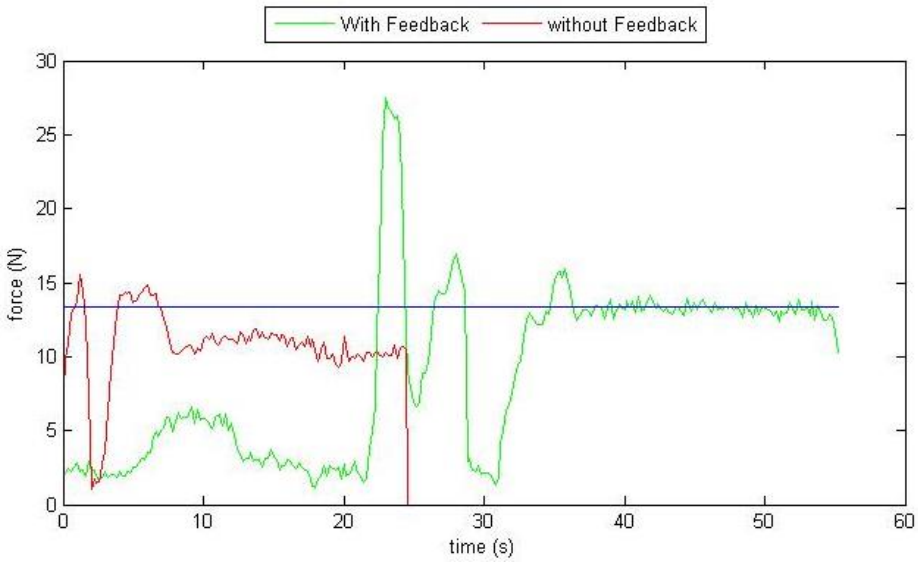


**Fig. 5.27: 7th subject using and not using visual feedback in the first try**

The results from the eighth untrained user shows that using the LCD feedback improved training. For example, in the third try, the user reached the target force after 5 seconds, which was slightly faster compared to the first two tries. Also, after having a sense of the amount of force needed, the target force was reachable even without feedback. Figures 5.28-30 show these outcomes.

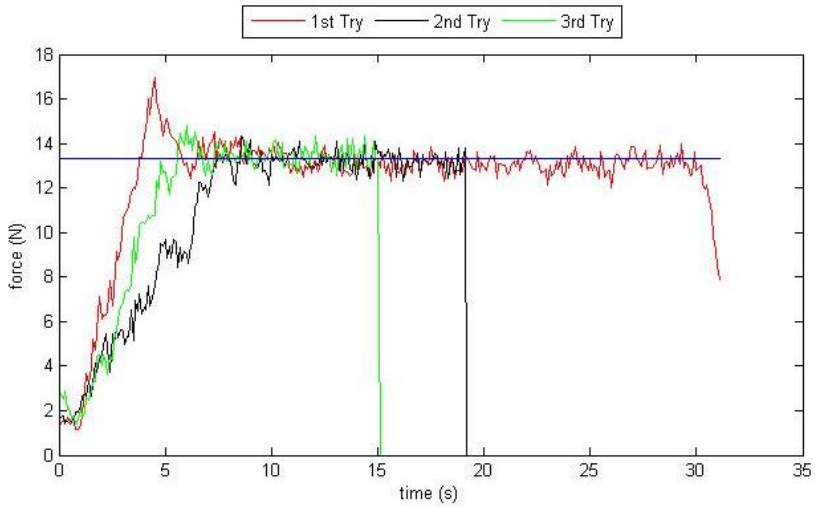


**Fig. 5.28: 8th subject using visual feedback**

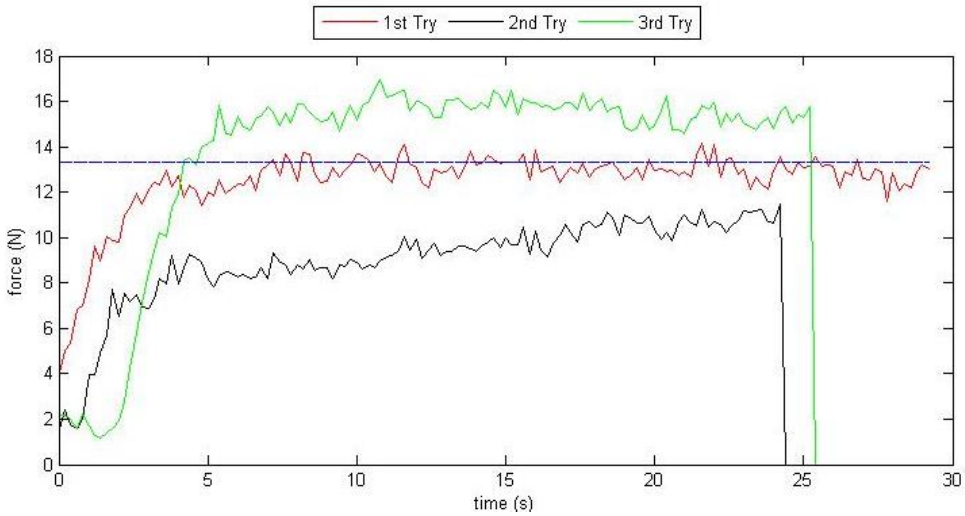


**Fig. 5.29: 8th subject not using visual feedback in three tries**

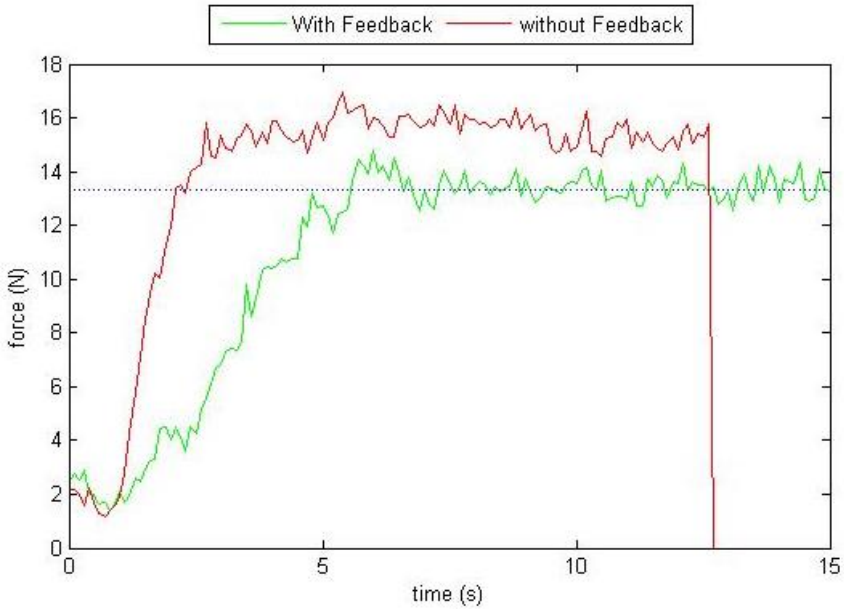


**Fig. 5.30: 8th subject using and not using visual feedback**

The ninth user testing the device with visual feedback took a long time to reach the target force on the first trial. However, the time decreased significantly after using the device two more times. Figures 5.31-33 illustrate these findings.

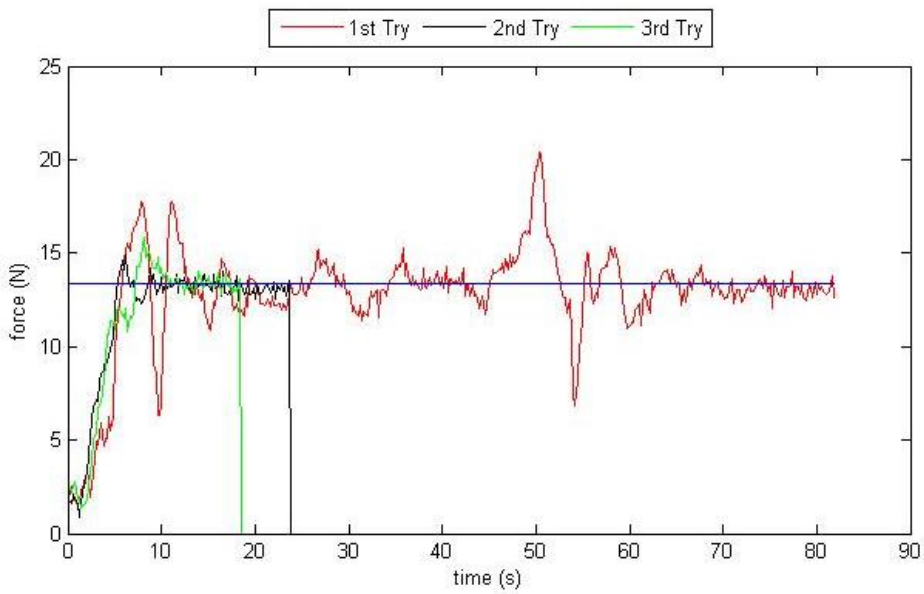


**Fig. 5.31: 9th subject using visual feedback repeated three times**

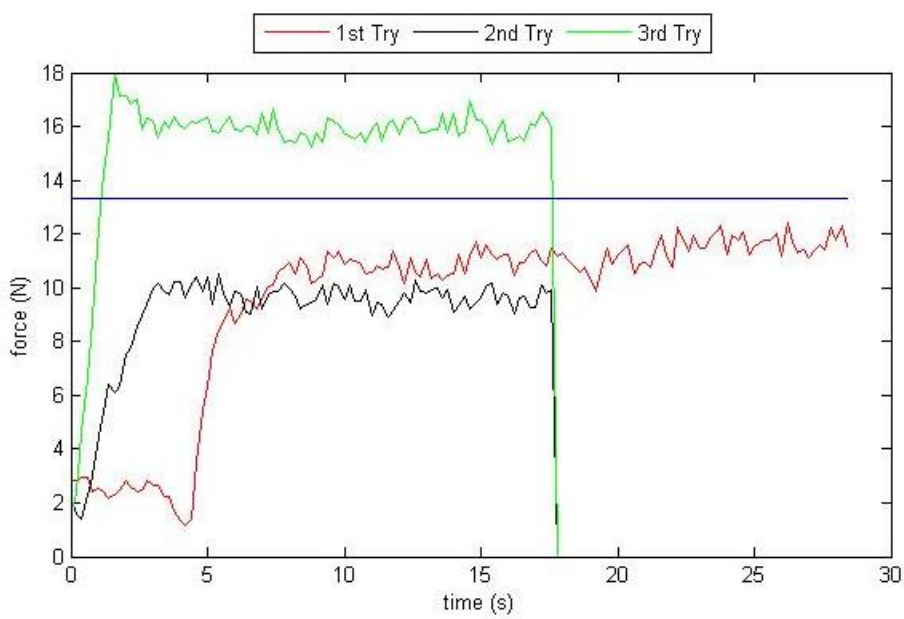


**Fig. 5.32: 9th subject not having visual feedback**

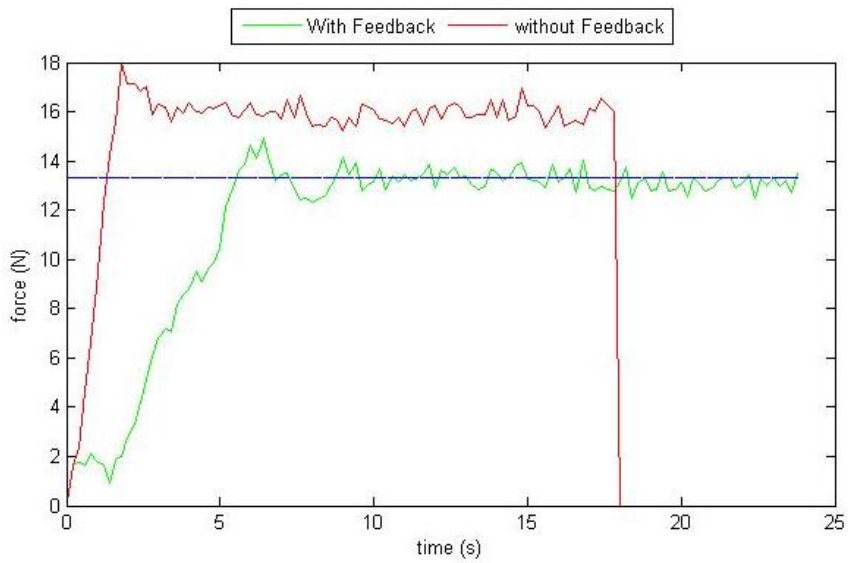


**Fig. 5.33: 9th subject using and not using visual feedback**

The time to reach the target force decreased by five seconds over three trials for our untrained tenth user (Figure 5.34). Also, the third time of trying the device without LCD feedback, the user could reach the target force. This shows that the device could give a sense of the target force. Figure 5.35 shows results of not using feedback, and Figure 5.36 compares with and without feedback.

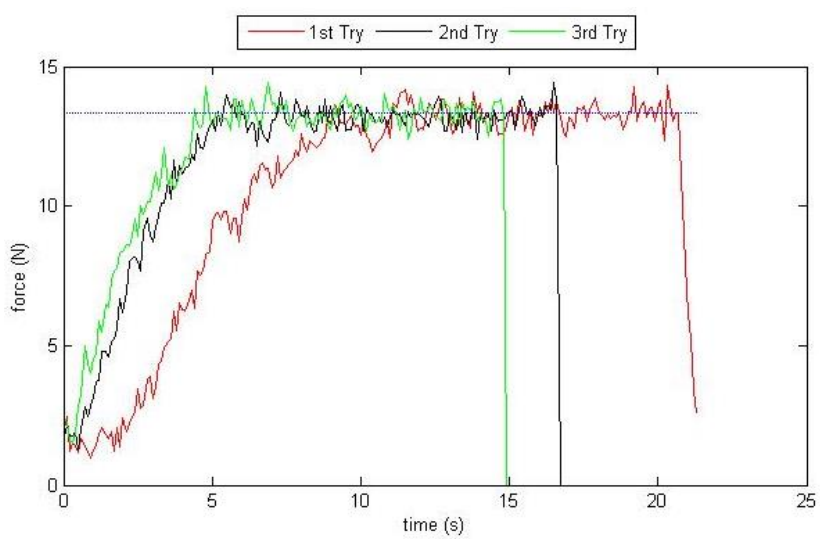


**Fig. 5.34: 10th subject using visual feedback repeated three times**

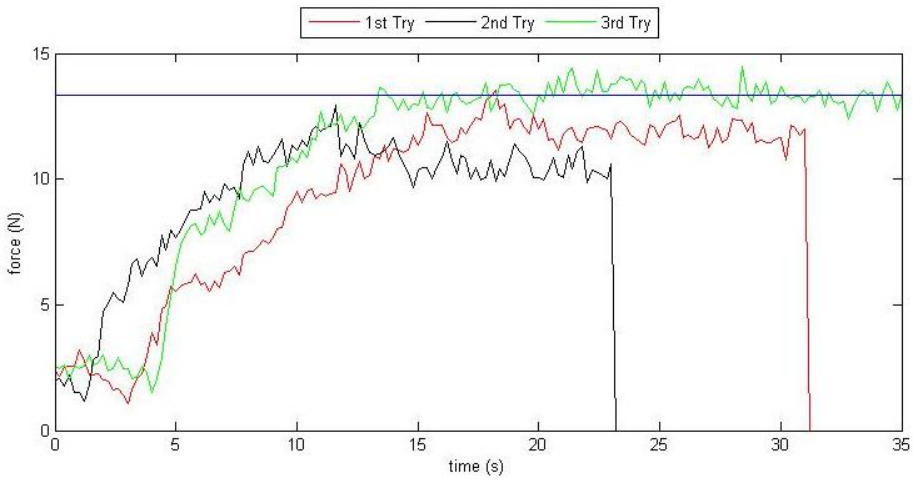


**Fig. 5.35: 10th subject not using visual feedback repeated three times**

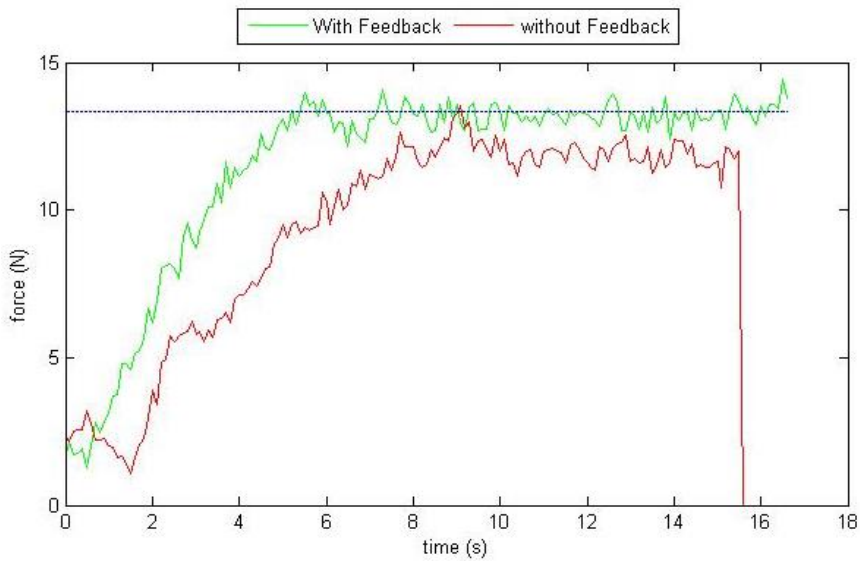


**Fig. 5.36: 10th subject using and not using visual feedback**

In summary, experiments have been done with 10 users, and the recorded data have been used to get the standard deviation. Comparison graphs were used to illustrate the efficacy of the LCD feedback. Each user held the device, and applied force to the phantom. The target force measured by the load cell was reached with and without the LCD feedback. They held the device at the target force for 10 seconds. A MATLAB code has been used to find the average error of the recorded data with respect to the target force (13.345 N) for all subjects using the LCD, and the average error with respect to the

target force for all subjects without using the LCD, and then a t-test has been used to compare these two groups to see if there is significant difference in reaching a target force with using this device with real-time visual feedback. The standard deviation data calculated from testing the device with visual feedback was near zero, showing that the force was held very consistently. The p-value for t-test calculated from standard deviation was 0.04757589. The t-test showed that the difference of using and not using the device is significant ($0.04757589 < 0.05$) in terms of steadiness of the force. Some MATLAB code has been used to plot graphs using one of the subjects to see if force accuracy improves. The target force was 13.345 N and the graphs show that using the LCD feedback can help to reach the target force. Also, repeating the experiments can help users apply more precise force with or without the LCD feedback. A t-test calculated from the means resulted in a p-value of 0.1170157. Although not conclusively significant, the ability to reach the target force is clearly better with visual feedback from the device.

Experiments have also been done to test the visual feedback of orientation of the ultrasound probe to see if having feedback improves holding the ultrasound probe in a precise position. Figures 5.37 and 5.38 illustrate the differences of using the LCD to get feedback to adjust the orientation of the probe. Target data for orientation specified to the subjects to reach during experiments is shown as a blue horizontal line. Qualitatively, the benefits appear similar to those for application of force.

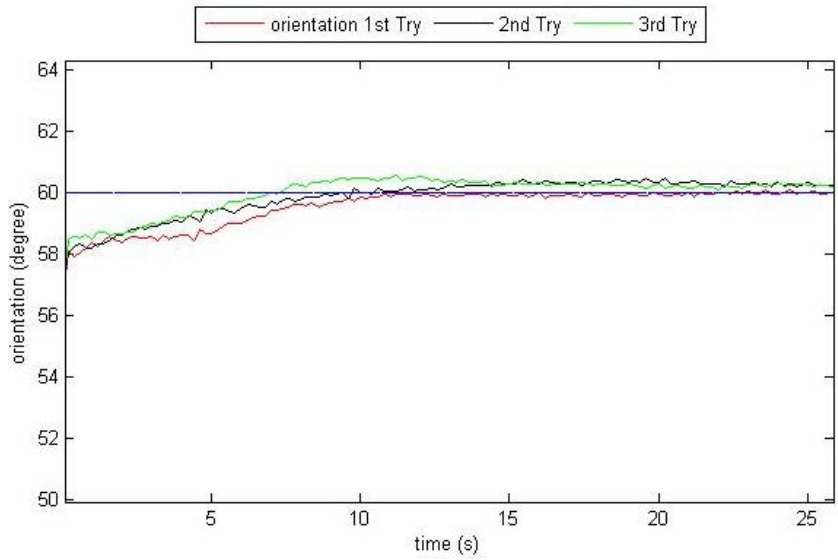


**Fig. 5.37: Using orientation visual feedback**

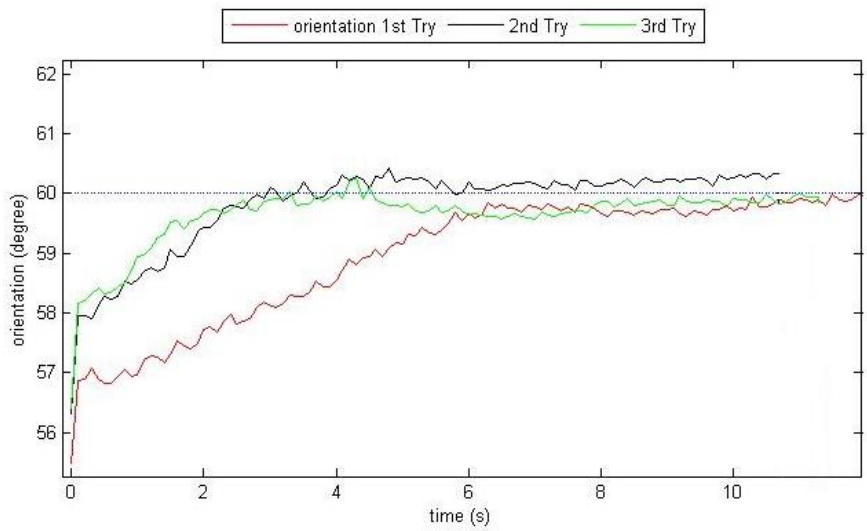


**Fig. 5.38: Not using orientation visual feedback**

# Chapter 6: Conclusion and Future Work

This thesis presents a new system for ultrasound training purposes with feedback features. A small system has been developed with the ability of displaying force and orientation to the operator during ultrasound training. A miniature load cell and an accelerometer have been used for these two measurements. The design was presented. The ability of the device to hold different types of ultrasound transducers makes it a multipurpose training tool.

Several experimental tests have been performed to verify the functionality of the device. Ten untrained randomly selected users participated in this work study. The force applied to a phantom made out of silicone was measured, and the orientation of ultrasound probe analyzed. A t-test computed from the standard deviation of data between two data groups of using LCD visual feedback and not using LCD visual feedback (0.04757589) indicate an improved efficacy of this device if implemented into current ultrasound training protocols.

One of the major points that are needed for future work is to get feedback from ultrasound technicians. Their comments after using and testing the device would provide valuable insights for potential improvements. Other phantoms could be constructed to replicate anatomic points of interest. Internal cavities, fluid, and objects can also be embedded within the phantom for landmark detection. These benchtop experiments can be used to improve the physical design of the device as well as the software and display to the user. Also, future work could include using semi-autonomous actuation to maintain a desired amount of pressure or force during ultrasonography.

# References


[1] Kramer, L. A., Sargsyan, A. E., Hasan, K. M., Polk, J. D., & Hamilton, D. R. (2012). Orbital and intracranial effects of microgravity: findings at 3-T MR imaging.*Radiology*, *263*(3), 819-827.

[2] Marshburn TH, Hadfield CA, Sargsyan AE, Garcia KM, Ebert D, Dulchavsky SA. New Heights in Ultrasound: First Report of Spinal Ultrasound from the International Space Station. Journal of Emergency Medicine. 2013 October 14; epub. DOI:10.1016/j.jemermed.2013.08.001. PMID: 24135505.

[3] Mader, T. H., Gibson, C. R., Pass, A. F., Kramer, L. A., Lee, A. G., Fogarty, J., ... & Polk, J. D. (2011). Optic disc edema, globe flattening, choroidal folds, and hyperopic shifts observed in astronauts after long-duration space flight.*Ophthalmology*, *118*(10), 2058-2069.

[4] Lakin, W. D., Stevens, S. A., & Penar, P. L. (2007). Modeling intracranial pressures in microgravity: the influence of the blood-brain barrier. *Aviation, space, and environmental medicine*, *78*(10), 932-936.

[5] Ren, R., Jonas, J. B., Tian, G., Zhen, Y., Ma, K., Li, S., ... & Wang, N. (2010). Cerebrospinal fluid pressure in glaucoma: a prospective study. *Ophthalmology*,*117*(2), 259-266.

[6] Jonas, J. B., & Wang, N. (2012). Association between arterial blood pressure, cerebrospinal fluid pressure and intraocular pressure in the pathophysiology of optic nerve head diseases. *Clinical & experimental ophthalmology*, *40*(4), e233-e234.

[7] Hawks, J. A., Twedt, M., Pfeifer, C., Spilinek, M., Ahlquist, E., Burger, M., ... & Bashford, G. (2015). Ocular Blood Flow Response to Applied Force: in vivo Tests Toward Noninvasive Intracranial Pressure Monitoring. *Journal of Medical Devices*, *9*(2), 020911.

[8] Ragauskas, A., Matijosaitis, V., Zakelis, R., Petrikonis, K., Rastenyte, D., Piper, I., and Daubaris, G., 2012, "Clinical Assessment of Noninvasive Intracranial Pressure Absolute Value Measurement Method," Neurology, 78(21), pp. 1684–1691.

[9] Mader, T. H., Gibson, C. R., Pass, A. F., Kramer, L. A., Lee, A. G., Fogarty, J., ... & Polk, J. D. (2011). Optic disc edema, globe flattening, choroidal folds, and hyperopic shifts observed in astronauts after long-duration space flight. Ophthalmology, 118(10), 2058-2069.

[10] Nelson, E. S., Mulugeta, L., & Myers, J. G. (2014). Microgravity-Induced Fluid Shift and Ophthalmic Changes.Life, 4(4), 621-665.

[11] Freudenrich, C. (2002). How ultrasound works.

[12] Salcudean, S. E., Bell, G., Bachmann, S., Zhu, W. H., Abolmaesumi, P., & Lawrence, P. D. (1999, January). Robot-assisted diagnostic ultrasound–design and feasibility experiments. In *Medical Image Computing and Computer-Assisted Intervention–MICCAI'99* (pp. 1062-1071). Springer Berlin Heidelberg.

[13] Cole, K. (2008). Sonography's expansion into space. Journal of Diagnostic Medical Sonography.

[14] Martin, D. S., South, D. A., Garcia, K. M., & Arbeille, P. (2003). Ultrasound in space. *Ultrasound in medicine & biology*, *29*(1), 1-12.

[15] Steinbach, G. C., Macias, B. R., Tanaka, K., Yost, W. T., & Hargens, A. R. (2005). Intracranial pressure dynamics assessed by noninvasive ultrasound during 30 days of bed rest. Aviation, space, and environmental medicine, 76(2), 85-90.

[16] Bhatia, A., & Gupta, A. K. (2007). Neuromonitoring in the intensive care unit. I. Intracranial pressure and cerebral blood flow monitoring. Intensive care medicine, 33(7), 1263-1271.

[17] The Brain Trauma Foundation. The American Association of Neurological Surgeons. The Joint Section on Neurotrauma and Critical Care (2000) Recommendations for intracranial pressure monitoring technology. J Neurotrauma 17:497–506

[18] Fogarty, J.A., Otto, C., Kerstman, E., Oubre, C., Wu, J. (2011). The visual impairment intracranial pressure summit report. NASA/TP-2011-216160.

[19] Masuda, K., Kimura, E., Tateishi, N., & Ishihara, K. (2001). Three dimensional motion mechanism of ultrasound probe and its application for tele-echography system. In *Intelligent Robots and Systems, 2001. Proceedings. 2001 IEEE/RSJ International Conference on* (Vol. 2, pp. 1112-1116). IEEE.

[20] Vieyres, P., Poisson, G., Courrèges, F., Mérigeaux, O., & Arbeille, P. (2003). The TERESA project: from space research to ground tele-echography.*Industrial robot: an international journal*, *30*(1), 77-82.

[21] Marshburn TH, Hadfield CA, Sargsyan AE, Garcia KM, Ebert D, Dulchavsky SA. New Heights in Ultrasound: First Report of Spinal Ultrasound from the International Space Station. Journal of Emergency Medicine. 2013 October 14; epub. DOI:10.1016/j.jemermed.2013.08.001. PMID: 24135505.

[22] Vilchis, A., Troccaz, J., Cinquin, P., Masuda, K., & Pellissier, F. (2003). A new robot architecture for tele-echography. *Robotics and Automation, IEEE Transactions on*, *19*(5), 922-926.

[23] Treece, G. M., Gee, A. H., Prager, R. W., Cash, C. J., & Berman, L. H. (2003). High-definition freehand 3-D ultrasound. Ultrasound in medicine & biology,29(4), 529-546.

[24] Hunter, I. W., Doukoglou, T., Lafontaine, S. R., Charette, P. G., Jones, L. A., Sagar, M. A., ... & Hunter, P. J. (1993). A Teleoperated Microsurgical Robot and Associated Virtual Environment for Eye Surgery. Presence, 2(4), 265-280.

[25] Dulchavsky, S. A., Sargsyan, A. E., Garcia, K. M., Melton, S. L., Ebert, D., & Hamilton, D. R. (2011). Intuitive ultrasonography for autonomous medical care in limited-resource environments. Acta Astronautica, 68(9), 1595-1607.

[26] Marshburn, T. H., Hadfield, C. A., Sargsyan, A. E., Garcia, K., Ebert, D., & Dulchavsky, S. A. (2014). New heights in ultrasound: first report of spinal ultrasound from the international space station. *The Journal of emergency medicine*, *46*(1), 61-70.

[27] Burcher, M. R., Noble, J. A., Man, L., & Gooding, M. (2005). A system for simultaneously measuring contact force, ultrasound, and position information for use in force-based correction of freehand scanning. *Ultrasonics, Ferroelectrics, and Frequency Control, IEEE Transactions on*, *52*(8), 1330-1342.

[28] Najafi, F., & Sepehri, N. (2008). A novel hand-controller for remote ultrasound imaging. *Mechatronics*, *18*(10), 578-590.

[29] Delgorge, C., Courrèges, F., Bassit, L. A., Novales, C., Rosenberger, C., Smith-Guerin, N., ... & Vieyres, P. (2005). A tele-operated mobile ultrasound scanner using a light-weight robot. *Information Technology in Biomedicine, IEEE Transactions on*, *9*(1), 50-58.

[30] Salcudean, S. E., Bell, G., Bachmann, S., Zhu, W. H., Abolmaesumi, P., & Lawrence, P. D. (1999, January). Robot-assisted diagnostic ultrasound–design and feasibility experiments. In Medical Image Computing and Computer-Assisted Intervention–MICCAI'99 (pp. 1062-1071). Springer Berlin Heidelberg.

[31] Conti, F., Park, J., & Khatib, O. (2014, January). Interface design and control strategies for a robot assisted ultrasonic examination system. In Experimental Robotics (pp. 97-113). Springer Berlin Heidelberg.

[32] http://www.dwl.de/index.php?art_id=enen2540b8be4516e569539c0f5d8515

[33] https://www.adafruit.com/products/1085

[34] https://www.kitronik.co.uk/blog/lm324-quad-op-amp-datasheet/

[35] https://en.wikipedia.org/wiki/Differential_amplifier

[36] http://users.ece.gatech.edu/mleach/ece4435/chap01.pdf

[37] https://www.adafruit.com/products/1085

[38] Burcher, M. R., Noble, J. A., Man, L., & Gooding, M. (2005). A system for simultaneously measuring contact force, ultrasound, and position information for

use in force-based correction of freehand scanning. *Ultrasonics, Ferroelectrics, and Frequency Control, IEEE Transactions on*, *52*(8), 1330-1342.

[39] http://www.ic0nstrux.com/FlexiForce-Sensor-Demo-Kit#!prettyPhoto

[40] Salcudean, S. E., Bell, G., Bachmann, S., Zhu, W. H., Abolmaesumi, P., & Lawrence, P. D. (1999, January). Robot-assisted diagnostic ultrasound–design and feasibility experiments. In Medical Image Computing and Computer-Assisted Intervention–MICCAI'99 (pp. 1062-1071). Springer Berlin Heidelberg.

[41] https://www.parallax.com/sites/default/files/downloads/30056-FlexiForce-Datasheet.pdf

[42] Ketchem, T., Twedt, M., Lim, D., Bashford, G., & Hawks, J. A. (2015). Proof-of-Concept Prototype for Noninvasive Intracranial Pressure Monitoring Using Ocular Hemodynamics Under Applied Force. Journal of Medical Devices, 9(2), 024502.

[43] Lindseth, F., Tangen, G. A., Langø, T., & Bang, J. (2003). Probe calibration for freehand 3-D ultrasound. Ultrasound in medicine & biology, 29(11), 1607-1623.

[44] Gilbertson, M., Anthony, B., & Sun, S. Y. (2010). Handheld Force Controlled Ultrasound Probe. Journal of Medical Devices, 4(2), 027540.

[45] http://www.futek.com/product.aspx?stock=FSH00091

[46] http://eeshop.unl.edu/ee_shop_store.html

[47] http://www.smooth-on.com/Silicone-Rubber-an/c2_1115_1130/index.html

# Appendix A. S-Beam Futek Load Cell Data Sheets

## FUTEK MODEL LSB200 (L2357)

Drawing Number: FI1041-D

| INCH [mm] | R.O.= Rated Output |
|---|---|

WIRING CODE (WC1)

| +Excitation | -Excitation | +Signal | -Signal |
|---|---|---|---|
| RED | BLACK | GREEN | WHITE |
| Shield | | | |
| FLOATING | | | |

## S-BEAM JUNIOR LOAD CELL

*DESIGNED FOR INLINE LOADING IN TENSION & COMPRESSION*
*AVAILABLE IN #4-40 AND M3x0.5 METRIC THREADS*

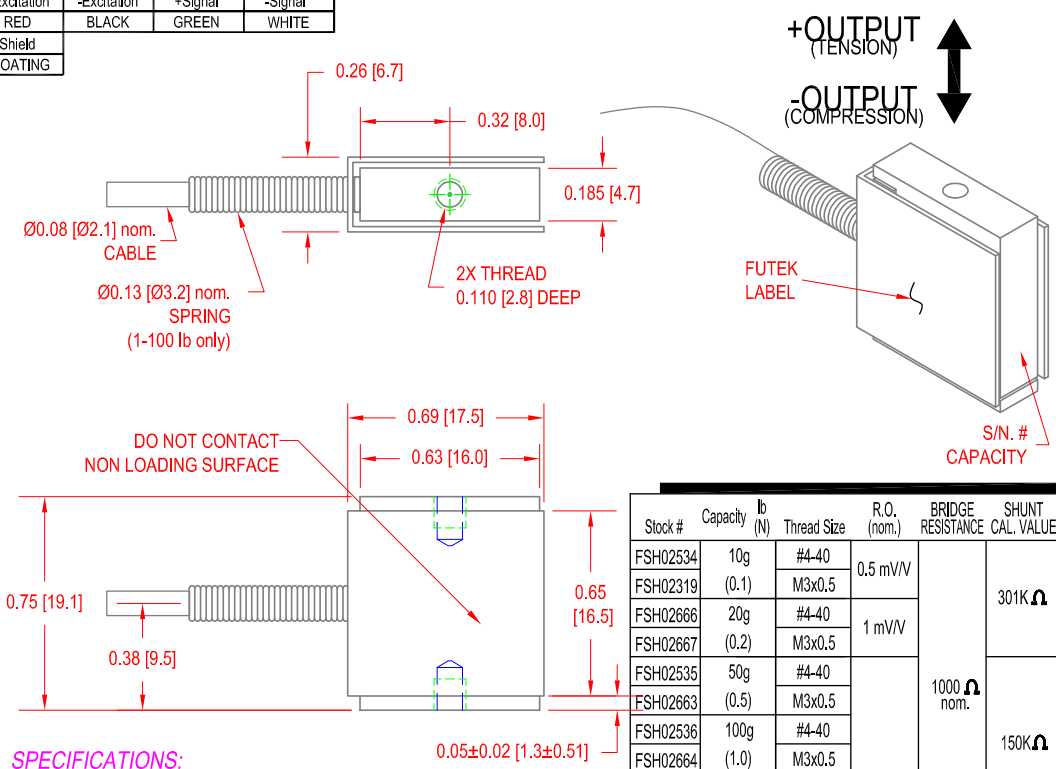


| Stock # | Capacity | lb (N) | Thread Size | R.O. (nom.) | BRIDGE RESISTANCE | SHUNT CAL. VALUE |
|---|---|---|---|---|---|---|
| FSH02534 | 10g | | #4-40 | 0.5 mV/V | 1000 Ω nom. | 301K Ω |
| FSH02319 | | (0.1) | M3x0.5 | | | |
| FSH02666 | 20g | | #4-40 | 1 mV/V | | |
| FSH02667 | | (0.2) | M3x0.5 | | | |
| FSH02535 | 50g | | #4-40 | 2 mV/V | | 150K Ω |
| FSH02663 | | (0.5) | M3x0.5 | | | |
| FSH02536 | 100g | | #4-40 | | | |
| FSH02664 | | (1.0) | M3x0.5 | | | |
| FSH02602 | 250g | | #4-40 | | | |
| FSH02665 | | (2.5) | M3x0.5 | | | |
| FSH00091 | 1 | | #4-40 | | 350 Ω nom. | 60.4K Ω |
| FSH00101 | | (4.5) | M3x0.5 | | | |
| FSH00092 | 2 | | #4-40 | | | |
| FSH00102 | | (8.9) | M3x0.5 | | | |
| FSH00093 | 5 | | #4-40 | | | |
| FSH00103 | | (22.2) | M3x0.5 | | | |
| FSH00095 | 10 | | #4-40 | | | |
| FSH00104 | | (44.5) | M3x0.5 | | | |
| FSH00096 | 25 | | #4-40 | | | |
| FSH00105 | | (111) | M3x0.5 | | | |
| FSH00097 | 50 | | #4-40 | | | |
| FSH00106 | | (222) | M3x0.5 | | | |
| FSH00098 | 100 | | #4-40 | | | |
| FSH00107 | | (445) | M3x0.5 | | | |

### SPECIFICATIONS:

| | |
|---|---|
| RATED OUTPUT | SEE CHART |
| SAFE OVERLOAD | 1000% of R.O. |
| | 200% of R.O. Tension Only (50-100 lb)* |
| ZERO BALANCE** | ±3% of R.O., ±5% of R.O. (10-20g) |
| EXCITATION (VDC OR VAC) | 10 Max |
| BRIDGE RESISTANCE | SEE CHART |
| NONLINEARITY | ±0.1% of R.O. |
| HYSTERESIS | ±0.1% of R.O. |
| NONREPEATABILITY | ±0.05% of R.O. |
| TEMP. SHIFT ZERO | ±0.01% of R.O./°F [0.018% of R.O./°C] |
| TEMP. SHIFT SPAN | ±0.02% of LOAD/°F [0.036% of LOAD/°C] |
| COMPENSATED TEMP. | 60 to 160°F [15 to 72°C] |
| OPERATING TEMP. | -60 to 200°F [-50 to 93°C] |
| MATERIAL | ALUMINUM (10g-10lb), STAINLESS STEEL (25-100lb) |
| WEIGHT | 0.3 oz [9 g] |
| DEFLECTION | 0.003-0.005 [0.07-0.13] |
| IP RATING | IP40 |

CABLE: #29 AWG, 4 Conductor, Spiral Shielded Silicone Cable, 5 ft [1.5 m] Long

ACCESSORIES AND RELATED INSTRUMENTS AVAILABLE

| | |
|---|---|
| CALIBRATION (STD) | 5 pt TENSION; SEE CHART FOR SHUNT CAL VALUE. |
| CALIBRATION (AVAILABLE) | COMPRESSION |
| CALIBRATION TEST EXCITATION | 5 VDC |

*SENSOR STRUCTURE CAN HANDLE HIGH OVERLOADS BUT #4-40 and M3x0.5 THREADS MAY LIMIT OVERLOAD AT HIGHER CAPACITY

** ZERO BALANCE IS BASED ON LAYING SENSOR ON ITS SIDE (THREADS HORIZONTAL)

FUTEK ADVANCED SENSOR TECHNOLOGY, INC.



10 THOMAS
IRVINE, CA 92618 USA
1-800-23-FUTEK (38835)

INTERNET:
http://www.futek.com

# Appendix B. S-Beam Futek Load Calibration Sheet

FUTEK
ADVANCED SENSOR TECHNOLOGY, INC

## Calibration Data

**Sensor Info**

Model ..... LSB200
Item # ..... FSH00093
S/N ..... 556707
Capacity ..... 5 lb

**Calibration Data**

Test Temp ..... 73.4 °F (23 °C)
Relative Humidity ..... 30.4 %
Excitation ..... 5.00 (Vdc)
Input Resistance ..... 351 (Ohms)
Output Resistance ..... 351 (Ohms)

direction: Tension

Rated Output ..... 1.899 (mV/V)
Linearity ..... 0.032 % of R.O.

**Data Points**

| Load | Output | Non-Lin Error (%) | Hysteresis (%) |
|---|---|---|---|
| **channel: 1** | | | |
| (lb) | (mV/V) | | |
| direction: Tension | | | |
| 0.000 | 0.0000 | 0.000 | |
| 1.000 | 0.3800 | 0.016 | |
| 2.000 | 0.7600 | 0.032 | |
| 3.000 | 1.1396 | 0.026 | |
| 4.000 | 1.5192 | 0.021 | |
| 5.000 | 1.8985 | 0.000 | |
| 0.000 | -0.0006 | | |

**Shunt Calibration**

| Shunt Value (K ohm) | Output ( ) | Load (lb) |
|---|---|---|
| **channel: 1** | | |
| direction: Tension | | |
| 60.4 | 1.443803 | 3.802 |

**Shunt Cal is placed across (-E)(-S)**

FUTEK Advanced Sensor Technology Inc. 10 Thomas Irvine CA. 92618 Tel: 1(800)23-FUTEK Fax: (949)465-0905